DESIGN OF POLYMERIC NANOPARTICLES FOR EDIBLE ANTIMICROBIALS AND CHEMICAL OXYGEN SENSORS

By

SHIWEN SUN

A thesis submitted to the

Graduate School – New Brunswick

Rutgers, The State University of New Jersey

in partial fulfillment of the requirements

for the degree of

Master of Science

Graduate Program in Chemical and Biochemical Engineering

written under the direction of

Dr. Nina C. Shapley

and approved by

_____

_____

_____

_____

New Brunswick, New Jersey

May, 2014

ABSTRACT OF THE THESIS

Design of polymeric nanoparticles for edible antimicrobials

and chemical oxygen sensors

by SHIWEN SUN

Thesis Director:

Dr. Nina C. Shapley

Research and development of nanoscale materials have received increasing attention due to the small size scales and large surface-volume ratios involved, and the associated changes in properties compared to those of bulk systems. This dissertation introduces the design of two types of polymeric nanoparticles, intended for edible antimicrobials or for chemical oxygen sensors.

Recent outbreaks of foodborne pathogens have attracted public attention to food safety. Due to healthy life style trends, there is a demand for the development of an efficient, biocompatible sanitizing method for fresh and fresh-cut produce. We have developed chitosan-based nanoparticles modified with antimicrobial agents in order to achieve potent antimicrobial activity. Nisin, a widely used food preservative, has been attached to

chitosan nanoparticles by electrostatic forces with a layer of anionic alginic acid in between. ε-poly-L-lysine, a natural and broad-spectrum antimicrobial, has been incorporated when forming chitosan nanoparticles. Particle properties have been studied, including the particle diameter, zeta potential, and morphology. Further investigation of antimicrobial activity is ongoing in Dr. Karl Matthews' group in the Department of Food Science, including determination of the minimum inhibitory concentration, bacterial viability monitoring assays, and application in food washing steps.

Oxygen is one of the most import analytes in the world due to its high relevance to living things. Determination of oxygen concentration has great importance in various fields. A series of new nanoparticle-based optical oxygen sensors were developed. The luminescent oxygen indicator dyes Pt(II)–5,15-di(pentafluorophenyl)-10,20-di(4-bromophenyl)porphyrin (PtTFPP), and Pt(II) meso-tetra(4-bromophenyl)tetra(tert-butyl)benzoporphyrin (PtTPTtBuBP) were covalently immobilized into two different conjugated polymers. The resulting polymers were rendered positively or negatively charged via chemical modification and were used to prepare oxygen-sensitive nanoparticles via a nanoprecipitation technique. This method improved the brightness of the oxygen sensor by a factor of 4-6. Efficient energy transfer was established from conjugated polymers to the oxygen indicator dye. Highly efficient two-photon excitation is expected. Different functional groups were also added to achieve adequate stability in aqueous dispersion and cell-penetration ability for different types of cells and tissues. Further investigation is ongoing in Dr. Dmitri Papkovsky's group at University College Cork (Ireland).

Acknowledgement

First and foremost, I would like to thank my advisor, Dr. Nina Shapley, for her valuable guidance and advice. I feel motivated and encouraged every time meeting with her. I am grateful for her constant support and understanding.

I am glad to work in Dr. Nina Shapley's group, with numbers of great colleagues and undergraduate students: Kun Yu, Kristin Steeley, Kapil Deshpandei, Anik Chaturbedi, Samyukta Budumuru, Nimish Patil, Chinmay Pathak, Adam Cham, Jenna Lo, Eric Somers, Sharif Farghaly,Vetri Velan.

I would like to express my thanks to our collaborators: Dr.Karl Matthews, Tsz-wai (Germaine) Tsui (Rutgers University, Food Science Department); Dr. Anubhav Tripathi, Glareh Azadi, James Park (Brown University, Biomedical Engineering). It was very nice working with them. And they always give me inspirational feedback.

Also I would like to thank everyone who supported and helped me during my research stay at Graz University of Technology in Austria: Dr. Ingo Klimant, Dr. Sergey Borisov, Dr. Torsten Mayr, all the group members in Dr. Ingo Klimant's group, Mag. Kathrin Manninger, Karin leber. And thank Dr. Yee Chiew for recommending me for this program. Thank the Marshall Plan Scholarship Austria for financial support.

No one walks alone on the journey of life. I am grateful to meet these best friends here: Yifan Wang, Zhixuan Su, Ji Long. You always cheer me up when I am down; share my happiness when I am elated. We are not only friends, we are more like families.

Last but not least, I would say my parents are my heroes. They understand me, support me, and encourage me to chase my dreams, without asking anything from me.

Contents

List of Figures

List of Tables

Chapter 1 Introduction

This master's dissertation is divided into two parts. Design of polymeric nanoparticles for edible antimicrobials is the research work I performed during my master's studies at Rutgers University from 2012 to 2014. The other part of the research work, on the design of polymeric nanoparticles for chemical oxygen sensors, was conducted during my research stay at Graz University of Technology in Austria from October 2013 to January 2014. The two kinds of polymeric nanoparticles are aim for biological application.

1.1 Motivation/ Significance

1.1.1 Design of polymeric nanoparticles for edible antimicrobials

Food safety is a continuous fight against human enteric pathogens to avoid the contamination of foods. About 1 in 6 (or 48 million) Americans become ill with a foodborne illness each year[1]. Microorganisms, particularly pathogenic non-spore forming bacteria, parasitic helminthes, and protozoa are usually considered the causes of the contamination of foods, which leads to an enormous public health problem[2]. Over the past several decades, researchers have developed and investigated various methods to reduce the microbiological load of produce, including physical, chemical, and biological methods. Despite this continuous dedication, there is an upward trend in the number of outbreaks of pathogenic bacteria contaminating widely consumed produce and causing serious disease nationwide-[3] and internationally [4]. According to the record of recalls of foods due to microbiological contamination classified by the U.S. Food and Drug

Administration from fiscal years 2003 through 2011, *Salmonella* (71%), *Listeria monocytogenes* (18%), *Clostridium botulinum*, and *Escherichia coli* O157:H7 are the four leading pathogens responsible for these food-related recall events[3].

Due to the trend of increasingly healthy diets in consumers' lifestyles and the progress of retail marketing, the demand for fresh and fresh-cut produce has increased steadily in the past decades. Defined by the International Fresh-cut Produce Association (IFPA), "*these products are defined as any fresh fruit or vegetable or combination thereof physically altered from its original form, but remaining in a fresh state.*" Besides the high nutrition, convenience and added value of fresh-cut produce, is also a growing source of outbreaks of foodborne illness in the United States[5]. Commonly used conventional methods to eliminate foodborne pathogens include thermal heating and pasteurization[6]. But such methods cannot be used in the processes of fresh-cut produce. Current processing methods include the using of chlorine as chemical sanitizer. But the residual chlorine is considered a second contamination. Some efforts have been made to develop new preservation techniques, including high pressure processing, irradiation and pulsed electric fields[7, 8]. The basic approach of these techniques is destruction of the bacterial cell wall.

The rapid development of nanotechnology allowed broad application in multiple areas, including medicine[9], the pharmaceutical industry[10], and materials engineering[11], among others. The food industry also benefits from this new technology, including the improvement of taste[12] and extension of shelf-life by using nano-sized preservatives[13].

We envision the development of "green nanoparticles" to reduce total bacteria populations during the cleaning process for fresh/ fresh-cut produce. Chitosan, one of the widely used nanoparticle base materials, attracts our interest due to its relevant features. It is an edible, biocompatible polymer, and is recognized as a GRAS (Generally Recognized As Safe) component. Molecular chitosan solution shows antimicrobial properties at high concentrations (around 20 mg/mL)[14]. Meanwhile, it is interesting that chitosan nanoparticles are significantly more efficient as a clustering agent compared to an equal mass of molecular chitosan in solution[15]. Chitosan nanoparticles combined with other antimicrobial agents, such as Nisin or ε- poly-L-lysine, may effect a synergistic treatment on bacteria, and lower the concentration needed for those antimicrobial agents or broaden the effective bacteria spectrum of antimicrobial agents.

Due to these reasons, in this research, we use chitosan as the base material to synthesize nano- or micro-sized particles, with decoration of antimicrobial peptides for cleaning fresh-cut produce.

1.1.2 Design of polymeric nanoparticles for chemical oxygen sensors

Oxygen is one of the most important chemical species on the earth, especially for human beings. Quantitative determination of oxygen content, both in the gas[16] and the liquid phase[17], is of great importance for various fields, for example, medicine, biology, food manufacturing, oceanography, and environmental monitoring.[18]. Based on the measurement method, oxygen sensors can be divided into three categories: electrochemical[19], optical[20-22], and chemical (Winkler titration[23]).

Optical oxygen sensors have received great attention recently due to their advantages over other methods: inexpensive, easily miniaturized, simple preparation, no electrical interference, and not oxygen consuming[20]. The major principle used for an optical oxygen sensor is the quenching of the luminescence of an indicator dye by molecular oxygen[24]. The typical layout for an optical oxygen sensor consists of a luminescent indicator dye immobilized in a polymeric matrix, and deposited on a solid support (planar waveguide, microtitre plate, or optical fiber)[25].

The application area is also a critical factor for the design of optical oxygen sensors. In recent years, great attention has been focused on the understanding of cellular function and processes taking place in both normal and abnormal cells and tissues[26]. In biological systems, oxygen, as a small gaseous analyte, diffuses rapidly in solution, in and out of the cell, and is present in vast excess in the environment[27]. Therefore, there is high demand for the development of an accurate oxygen sensor which is versatile, flexible and simple. To satisfy these requirements, the ideal sensor should have high signal intensity, ability for cell penetration, suitability for ratiometric two-wavelength measurement, and potential for two-photon absorption, simple preparation and low working concentrations. Several kinds of particle based cellular/ intracellular oxygen sensors have been presented by scientists [27-32], which meet some of the requirements.

In this work, we present a series of conjugated polymer-based oxygen-sensitive nanoparticles, with high signal intensity under dual emission for ratiometric measurement, with functional groups aiding water dispersibility and cell penetration.

In Chapter 2, the methodology of edible antimicrobial particle synthesis and characterization is provided, and the microbiological assays that were performed in order to investigate the antimicrobial properties of chitosan-based nanoparticles. Chapter 3 mainly focuses on the design, synthesis and characterization of conjugated polymer-based oxygen-sensitive nanoparticles. Further investigation of the sensor application in a biological system is ongoing in Dr. Dmitri Papkovsky's group at University College Cork (Ireland). Chapter 4 discusses conclusions and recommendations for future work.

1.2 Background of polymeric nanoparticles for edible antimicrobials

1.2.1 Chitosan and alginate

Chitosan, α(1-4)2-amino 2-deoxy β-$_D$ glucan, is a deacetylated form of chitin, an abundant polysaccharide widely found in crustacean shells. The chemical structure is shown in Figure 1-1. Chitosan is positively charged due to the prevalence of amine groups that are protonated at low pH. With hydrosolubility, chitosan is able to interact with negatively charged polymers, macromolecules, and microorganism in an aqueous environment. Over the past two decades, chitosan has been well investigated as a material for drug delivery and biomedical applications [33-35]. Also, chitosan's unique properties in adsorbing heavy metal ions from industrial chemical waste streams make it as a promising biosorbent for water purification[36-38]. Further applications of chitosan in the food industry have been explored based on its biocompatibility and low toxicity [39-42]. Moreover, chitosan has been attracting great attention from researchers due to one of its most interesting properties: antimicrobial activity [15, 43-45].

The antimicrobial activity of chitosan towards Gram-negative bacteria is considered to result from its chemical and structural properties. The high positive charge of the amino group of chitosan at low pK_a value creates a polycationic structure, which can interact with the predominantly anionic components (lipopolysaccharides, proteins) of the Gram-negative surface[46]. Binding of polycationic molecules has been shown to disrupt the integrity of the outer membrane resulting in loss of the barrier function but lacking direct bactericidal activity. Generally, the antimicrobial activity of chitosan can be described as

the binding of cationic chitosan on the anionic cell surface of Gram-negative bacteria causing changes in permeability. Furthermore, the permeabilizing effects were demonstrated at slightly acidic conditions (pH 5.3) in which chitosan is protonated; and at this pH, the carboxyl and phosphate groups of the bacterial surface are anionic and offer potential sites for electrostatic binding of chitosan[14].

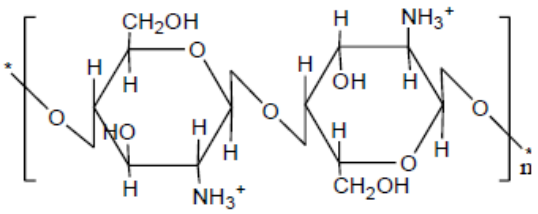

Figure 1-1 Chemical structure of chitosan.[47]

Tripolyphosphate (TPP) is a non-toxic polyanion, which is suitable for food industry applications. The protonated amine groups in chitosan interact with the negatively charged counterion, TPP, through an electrostatic interaction, and ionic cross-linked networks are created[47, 48] (see Figure 1-2).

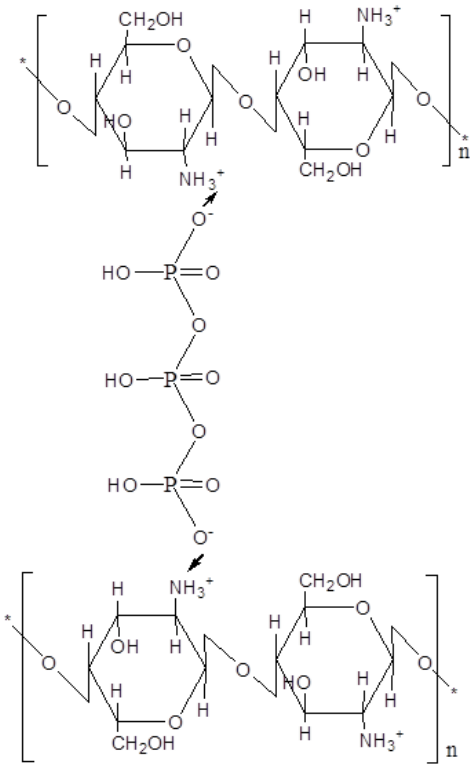

Figure 1-2 Cross-linking of chitosan with tripolyphosphate (TPP)[47].

Alginate is a linear, anionic copolymer consisting of two subunits, mannuronic acid (M block) and guluronic acid (G block) (see Figure 1-3). Alginate is extracted from brown algae. Due to its favorable properties, since it is biocompatible[49], non-toxic, non-immunogenic and biodegradable[50], alginate has been widely used as a biomaterial in various areas, such as cell immobilization[51], drug delivery[52], controlled release[53], water purification[36], as well as in food applications[54]. A number of free hydroxyl and carboxyl groups make alginate versatile for different chemical modifications to yield more alginate derivatives.

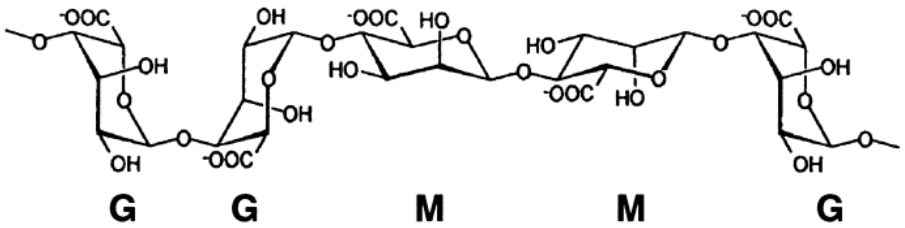

Figure 1-3 Chemical structure of alginate.[55]

1.2.2 Nisin and ε- poly-L-lysine

Nowadays, various kinds of antimicrobial agents have been widely used in different fields, for example chlorhexidine, triclosan, and xylitol. However, these antibacterial agents have certain drawbacks, such as drug resistance or poor solubility[56].

Nisin, produced by *Lactococcus lactis*, is a 34-residue peptide (see Figure 1-4). It is a broad-spectrum antimicrobial substance, targeting Gram-positive and Gram-negative microorganisms[57]. Also, nisin is a 3.5 kDa cationic amphiphilic peptide with a net positive charge[58]. Since it has been identified as Generally Recognized as Safe (GRAS) by the FDA since 1988[59], Nisin has been widely used as a food antimicrobial agent to extend the shelf life of beverages, meat, and dairy products[60]. The mechanism of Nisin against bacteria is by forming pores to interfere with cell wall biosynthesis which leads to bacterial apoptosis[61]. Other advantages of Nisin are that it does not produce drug resistance or chiasmatic resistance and it is non-toxic, odorless, colorless and tasteless[62].

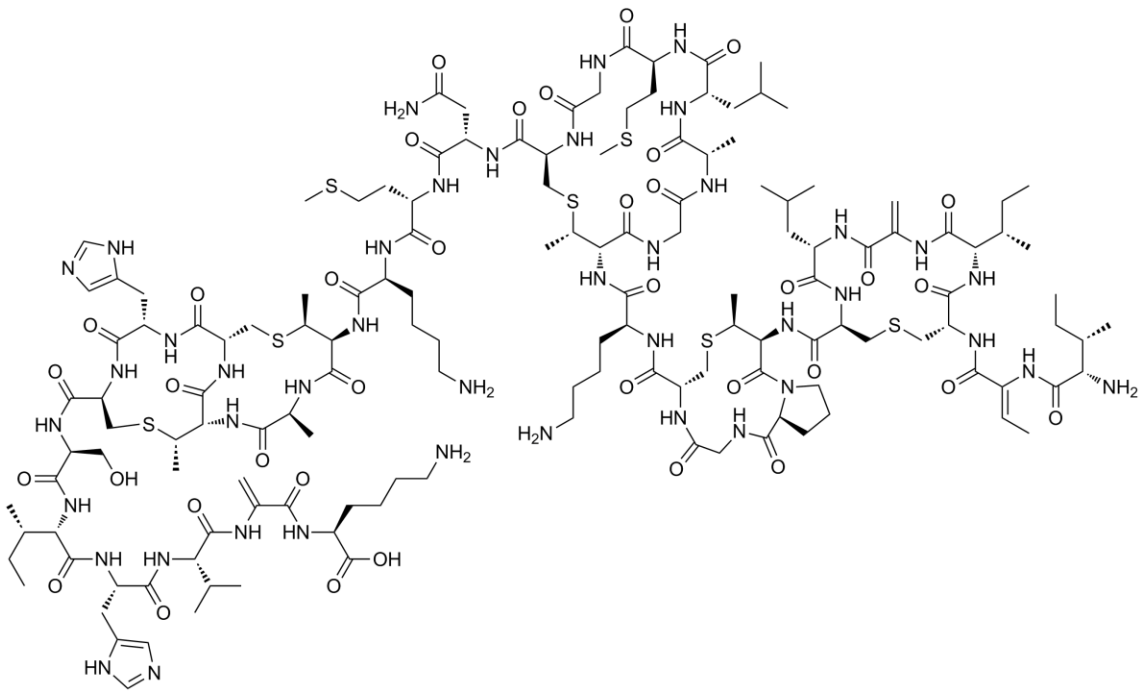

Figure 1-4 Chemical structure of Nisin. [57]

ε- poly-L-lysine, synthesized in aerobic bacterial fermentation by *Streptomyces albulus*, is a homopolymer of L-lysine, consisting of about 25-30 units of the amino acid lysine (see figure 1-5). These lysine molecules are linked by their epsilon amino groups and carbonyl groups, unlike normal peptide bonds which are linked by alpha-carbon groups, which is why this polymer has epsilon (ε) in its name[63]. Since it has been approved for food use in Japan in 1987[64], ε- poly-L-lysine has a long history of use as a preservative in various foods, such as fish, potato salad, steamed cakes, and Japanese beef steak. ε-poly-L-lysine functions as an antibacterial agent by stripping away the bacteria's outer membrane and causing leakage of cellular contents[65].

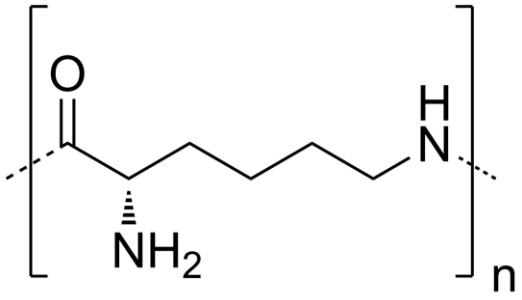

Figure 1-5 Chemical structure of ε- poly-L-lysine[63].

1.2.3 Chitosan nanoparticles applications

Due to the unique polymeric and cationic character, chitosan nanoparticles have been well investigated for different applications[66]. Among these applications, the pharmaceutical industry is definitely the one most in favor of chitosan nanoparticles. With the advantage of a high ratio of surface area to volume, chitosan nanoparticles have attracted great attention in targeted drug delivery. To utilize this versatile hydrogel material to make nanoparticles as carrier for drugs, protein, and DNA, different methods have been investigated by several workers [67-70].

Another property of chitosan, adsorbing heavy metal ions from industrial chemical waste streams, received attention for utilizing chitosan nanoparticles for water purification applications as well. A systematic study has been performed by our group member Kun Yu on the topic of copper ion adsorption by chitosan gel nanoparticles and calcium-alginate gel beads for water purification applications.[36]

1.2.4 Previous work of chitosan-based nanoparticles

In this study, chitosan nanoparticle synthesis has been optimized in order to maximize antimicrobial properties. A smaller than 1:5 concentration ratio of TPP:chitosan was used during the preparation of chitosan nanoparticles. Through TEM images, we observed that the lower concentration ratio yields a better spherical shape of the chitosan nanoparticles compared to the standard 1:5 concentration ratio. Also, these TPP-lean particles were produced in order to observe the effect of the degree of cross-linking on the properties of the nanoparticles and the resulting adsorption capability[36].

The size and surface charge of chitosan nanoparticles can be tailored by alginate coating. Particle diameter and the change in surface charge of chitosan nanoparticles increase along with the increase of the mass ratio of chitosan and coated alginate[71]. This study enables us to have a better knowledge during the modification of chitosan nanoparticles for interaction with other species.

Chitosan nanoparticles also have demonstrated strong and spontaneous interactions with gram-negative bacteria. The concentrations of nanoparticles and bacteria play a role in the size and cohesion of the bacteria-nanoparticle cluster. The whole aggregation process has been observed to happen rapidly, within seconds of mixing, by optical density measurements. And this feature was only noticed in the nanoparticle configuration, and is much less pronounced in molecular chitosan[15].

Chitosan nanoparticles also show synergistic action with a low electric field to improve antimicrobial potency. Chitosan nanoparticles did not show significant ability to inhibit bacteria alone. The combination of chitosan nanoparticles and a sustained electric field

successfully reduced bacteria viability by 2 – 2.5 orders of magnitude. The voltage needed to reduce same amount of bacteria was much higher, by about an order of magnitude, than the voltage used in combination with chitosan nanoparticles[45].

For the application in food industry, molecular chitosan has been used as novel preservative or a coating material for fruits and vegetables[43, 72]. Chitosan nanoparticles have been mainly investigated as drug delivery systems in the pharmaceutical industry[73]. Some applications used a chitosan-based nanoparticles film as a packing material[74].

1.3 Background of polymeric nanoparticles for chemical oxygen sensors

Optical sensors, or opt(r)odes, are a group of chemical sensors in which utilizing electromagnetic radiation to generate analytical signals. The change of a specific parameter is used to interpret the interaction between the radiation and the sample[75]. Generally, an optical sensor consists of a chemical recognition unit (sensing element or receptor) and a transduction unit (transducer). The receptor produces the optical signal proportional to a certain parameter (e.g. the concentration of a given compound, pH, etc.). Then the transducer translates the optical sensor for processing[18, 76]. If the receptor is produced by synthesis, it is called "chemosensor". And "biosensor" defines sensors with a receptor consisting biological substance (e.g. enzymes, immunoglobulins, etc.)[77].

There are two main categories of optical sensors: intrinsic optical sensor and extrinsic optical sensor. An intrinsic optical sensor is only responding to the certain parameter of the analyte. An extrinsic optical sensor produces optical signals corresponding to the interaction of the analyte and the indicator, while the analyte itself doesn't generate any signals.

Optical sensors have been used widely in different fields, including biomedical research[78], marine biology[79], biological and toxicological screening[80, 81], and food packing[82], for measurements of oxygen, CO_2, NH_3, pH and other ionic species.

1.3.1 Design of an optical sensor

Normally, an optical sensor at least consists of two units: an optical detection system and immobilization system. The detection system can be direct sensing or indicator-mediated

sensing. For directing sensing, the analyte can be measured directly by some intrinsic optical property (e.g. absorption, luminescence). While the indicator-mediated sensing system, the analyte concentration or other properties is monitored by an intermediate agent, usually an analyte-sensitive dye (indicator), to present as optical change[24, 83].

Immobilization of the indicator also plays important role in the design of optical sensor. There are three approaches used widely.

Impregnation – apply physical absorption, chemisorption or electrostatic bonding to immobilize the indicator to the polymer matrix[18].

Covalent bonding – the indicator is covalently bonded to the polymer matrix[84, 85].

Doping – the indicator is entrapped in the matrix during the polymerization process, where the indicator is simply mixed to the polymer stock solution[85].

1.3.2 Optical oxygen sensors

Among various optical sensors, oxygen sensors are widely used and well developed. The principle of optical oxygen sensors is dynamic quenching of the luminescence of indicator by molecular oxygen, which shortens the lifetime of the indicator. The triplet state is oxygen's ground state. Typically, the indicator is immobilized in an oxygen permeable polymer matrix[20].

This polymeric matrix acts as a solvent for the indicator and helps it to remain at the same concentration. Also, the matrix protects the indicator from ions or other species. The sensitivity of the sensor depends on the gas permeability of the matrix, and indicator

decay time. The permeability of oxygen to the matrix depends on the diffusion constant and the solubility coefficient. Commonly used materials for matrix are organic glassy polymers (e.g. polystyrene, poly(methylmethacrylate), fluorinated polymers, cellulose derivatives) and inorganic polymers (e.g. silicones and sol gels)[86]. Some materials' permeability coefficients are listed in table 3-1.

Table 1-1 Permeability rates of commonly used sensor matrices[20]

Polymer matrix	**Permeation rate for oxygen [$cm^2s^{-1}mmHg^{-1}$]**
Poly(methylmethacrylate)	9
Polystyrene	2.63
Polyvinylchloride	0.34
Poly(2,2,2-trifluoroethylmethacrylate)	32
Ethylcellulose	11.0
Cellulose acetate	5.85
Poly(dimethylsiloxane)	695

The relation of indicator lifetime and oxygen concentration can be described in Stern-Volmer-Plot (see Eq. 2-7). However, this is for the ideal case when the indicator distributes evenly on the matrix and has same accessibility to be quenched by molecular oxygen.

The immobilization of the indicator to the matrix is heterogeneous, and it is more suitable for the Two-Site-Model, which assumes two different quenching domains (see Eq. 1-1)[87].

$$\frac{I_0}{I} = \frac{1}{\frac{f}{1+K_{SV1}[O_2]} + \frac{1-f}{1+K_{SV2}[O_2]}}$$ Eq. 1-1

To simplify this model, assume that quenching is only possible in one of the two domains.

This is a rather unrealistic assumption but reduces the fit parameters to two and still fits well for many practical applications (see Eq. 1-2).

$$\frac{I_0}{I} = \frac{1}{\frac{f}{1+K_{SV1}[O_2]} + \frac{1-f}{1}}$$ Eq. 1-2

1.3.3 Indicators for optical oxygen sensors

The selection of optical oxygen sensors indicator dyes depend on the area of application, consequently, the matrix material and detection method. For example, applications of measuring oxygen in live cells and in tissues, it is necessary to consider the autofluorescence generated by biological substances, like proteins, DNA, and melanin. To minimize the absorption and scattering of the excitation and emission light in the tissue, it is more likely to employ indicators that have longwave-shifted absorption (590 – 650 nm) and emission (730 – 900 nm) bands[88, 89].

There are two main groups of optical oxygen sensors: absorption- and luminescence-based indicators. To date, luminescence-based indicators are most widely used in different fields of science. Also luminescent indicators can be classified into several groups: polycyclic aromatic hydrocarbons, polypyridyl complexes, metal porphyrins, syslometallated complexes, and complexes with rarely used central atoms. Among them, Pt(II) and Pd(II) are the most common used luminophores, due to their properties of

strong phosphorescence at room temperature, moderate to high molar absorption coefficients, large Stokes' shifts, relatively long phosphorescence lifetime, variation in spectral properties, and the possibility of synthetic modification to introduce the required functionalities. Many researchers have been working on Pt(II) and Pd(II) porphyrin complexes to improve the photophysical properties to make it more suitable for oxygen sensing in different areas and conditions[25].

1.3.4 Conjugated polymers

Conjugated polymers are organic macromolecules which consist at lease of one backbone chain of alternating double- and single-bonds. The interest increased regarding conjugated polymers due to the substantial π-electron delocalization along their backbones, which gives them conducting[90] and nonlinear optical properties[91-93]. These properties make conjugated polymers practical materials for applications in information storage, optical signal processing, batteries, and solar energy conversion[94].

Furthermore, electroluminescence from conjugated polymers makes it even more popular for rapidly expanding application areas[95, 96]. This luminescence efficiency is related to the delocalization and polarization of the electronic structure. It is a main advantage of conjugated polymers used as sensor materials over other materials that the conjugated polymers exhibit collective properties that are sensitive to very small perturbations[97]. For example, some work has been done to integrate conjugated polymers and porphyrins in one system as oxygen sensor[31, 98].

1.3.5 Oxygen-sensitive nanoparticles

Oxygen sensors can be realized in different forms, like planar optodes, fiber sensors, sensor paints, and microsensors. A nanoparticle-based oxygen sensor attracts more attention for its higher signals at lower oxygen levels[30], which is suitable for low concentration oxygen measurement for imaging and dynamic monitoring in intracellular or extracellular environments. Also due to its small size, inert matrix, and biocompatibility, the nanoparticle sensor is not physically disruptive to the surroundings[99], and can be applied for non-invasive real-time measurements[26, 27, 100].

Chapter 2 Synthesis and characterization of edible chitosan-based antimicrobial nanoparticles

2.1 Introduction

Food safety issues have attracted more and more attention recently. Since people are pursuing a healthier life style, fresh and fresh-cut produce are more likely to be chosen by customers. In the meantime, worldwide outbreaks of pathogenic bacteria involving contamination with several bacteria strains, including *Escherichia coli* O157:H7 and *Salmonella*, have been reported by the media for causing serious disease. Researchers have always been seeking and developing a more efficient and effective way to destroy multiple types of bacterial pathogens for use in various areas of the food industry.

Chitosan is a nontoxic, biocompatible, edible, GRAS (Generally Recognized As Safe) material, widely found in crustacean shells[39]. Many studies have focused on chitosan for applications in different areas, including drug delivery[33] and water purification[36]. Also chitosan-based nanoparticles show the potential ability as antimicrobial additives[43] and initiators for clustering[45].

In this work, we designed, synthesized, and characterized a series of chitosan-based nanoparticles with or without antimicrobial agents attached.

2.2 Experimental methods

2.2.1 Materials

Chitosan (low molecular weight) (CAS # 9012-76-4) was purchased from Sigma-Aldrich (St. Louis MO). It has a deacetylation degree of 90.85% and molecular weight range of 50 to 190 kDa. More specifically, the acquired batch has a viscosity of 185 cP (for a concentration of 1 w/w in 1 w/w acetic acid solution) (data provided by supplier). Sodium tripolyphosphate (TPP) was purchased from Sigma-Aldrich (St. Louis, MO).

Alginic acid (CAS # 9005-38-3) was purchased from Acros Organics (Morris Plains, NJ). It has a molecular weight range of 450 to 550 kDa, a viscosity of 485 cP (for a 1% w/w solution) (data provided by supplier). Additionally, the alginic acid consists of 65 – 75% guluronic acid (G) subunits and 25 – 35% mannuronic acid (M) subunits.

Nisin was provided by Danisco USA, Inc., under the trade name Nisaplin. Nisaplin is composed of minimum 1000 IU Nisin per mg of the product (2.5 %), with minimum 50% sodium chloride (by weight). ε-poly-L-lysine was received as gift from JNC Corporation (under the former name, Chisso). ε-polylysine was received as a stock solution containing 25% ε -poly-L-lysine (250 mg/mL) (Lot #2090501; Rye, NY).

Water used for all experiments was acquired from a Milli-Q water system.

2.2.2 Preparation of particles

Three types of chitosan-based nanoparticles were prepared in this work. The first type is plain chitosan nanoparticles, which simply followed the protocol from previous work of

the group[36]. The other two kinds of chitosan-based particles are modified by having Nisin or Polylysine incorporated. We name them, “CS with Nisin” and “CS&PL nanoparticles.”

Plain Chitosan Nanoparticles (CS NPs)

Plain chitosan-based nanoparticles were prepared following the well-established chitosan nanoparticle preparation protocol, involving ionic gelation interactions between chitosan and TPP with slight optimization. Chitosan solution (0.2 wt%, 2 mg/ml) was prepared by dissolving chitosan in water with an amount of acetic acid 1.75 times the mass of the chitosan. TPP solution was prepared by dissolving TPP in water to a concentration of 0.2 wt% (2 mg/ml). 0.7 ml of TPP solution (2 mg/ml) and 0.3 ml of DI water were added dropwise into 5 ml of chitosan solution (2 mg/ml) while stirring in a 20 ml vial. The mixture was kept stirring for another 30 min and then sat overnight in order to reach equilibrium. On the next day, the mixture was centrifuged for 30 min at 48,400 g (20,000 rpm) (Avanti J-E, Beckman Coulter, Brea, CA). The wet pellet was washed several times by DI water, dried, and weighed. Then it was redispersed in DI water by probe sonication (Misonix Sonicator 3000) for approximately 30 s. The wet mass of the pellet produced from each batch ranges from 0.15 g to 0.35 g, and the final concentration of the chitosan suspension ranges from 25 – 35 mg/ml. In previous experiments, the swelling ratio of the nanoparticles (wet mass / dry mass) was measured to be 18.44[36].

Nisin coated Chitosan Nanoparticles (CS NPs with Nisin)

Following the procedure of plain chitosan nanoparticle synthesis, a layer of alginic acid was coated on the surface in order to switch the surface charge of the particles to a

negative value. Alginate solution was prepared by dissolving alginic acid in DI water to a concentration of 0.1 wt% (1.0 mg/ml). 1:1 volume ratio of plain chitosan nanoparticle suspension (resulting from the procedure described in the previous section) and alginate solution was mixed together while stirring on a magnetic stir plate. The mixture was left overnight after an additional 30 minutes stirring to reach equilibrated state. On the next day, a similar washing step was applied. The nanoparticles were centrifuged at 48,400 g (20,000rpm) for 30 min, and washed, weighted, and redispersed in a certain amount of DI water so that the concentration of nanoparticles was approximately 20 mg/ml.

After the surface charge has been turned to a negative value, a layer of Nisin, which is cationic, was attached to the surface by electrostatic bonding. Nisin solution (0.1 wt%, 1 mg/ml) was prepared by dissolving Nisin in water with an amount of acetic acid of 1.75 times the mass of chitosan. The acetic acid added here helped Nisin to dissolve better and stay stable in DI water by lowering the pH. Just as in the alginate coating procedure, Nisin solution was mixed with the nanoparticle suspension at 1:1 volume ratio. The mixture was stirred for 30 minutes and left overnight to reach equilibrium, and the washing step was repeated the next day. After being redispersed in DI water, the final suspension of Nisin coated chitosan nanoparticles was obtained with a concentration of approximately 20 mg/ml.

Chitosan and Polylysine Nanoparticles (CS&PL NPs)

This type of nanoparticles was prepared in by a slightly different method. Instead of trying to coat polylysine on the outside of plain chitosan nanoparticles, polylysine was incorporated inside while forming the chitosan nanoparticles. Polylysine was obtained as

a stock solution at a concentration of 250 mg/ml. Chitosan was dissolved in DI water with a certain amount of polylysine stock solution added in order to achieve a mass ratio of 10:1 of chitosan and polylysine. Acetic acid was added to adjust the pH of the chitosan and polylysine mixture solution to 3.5 – 4. This chitosan and polylysine mixed solution was used to synthesize nanoparticles instead of chitosan solution. 0.7 ml of TPP solution (2 mg/ml) and 0.3 ml of DI water were added dropwise into 5 ml of chitosan and polylysine mixed solution (2 mg/ml total polymer concentration) while stirring. The mixture was kept stirring for another 30 min and sat overnight to reach equilibrium. On the next day, the mixture was centrifuged for 30 min at 48,400 g (20,000 rpm). The wet pellet was washed several times by DI water, dried, and weighed. Then, it was redispersed in DI water by probe sonication for approximately 30 s. The wet mass of the pellet produced from each batch ranged from 0.2 g to 0.3 g, and the final concentration of the chitosan suspension was approximately 20 mg/ml.

2.2.3 Characterization of particles

The zeta potential and size distributions of the three types of chitosan-based nanoparticles were characterized by using a Zetasizer Nano-ZS90 (Malvern Instruments, Malvern, UK). Dynamic light scattering was performed to measure the size distribution. And phase analysis light scattering was used to accomplish the zeta potential measurement. Zeta potential indicates the strength of electrostatic interparticle interactions. High zeta potential values confer stability, where the suspension resists aggregation. Each sample was sonicated to ensure that it was evenly suspended before characterization. Each sample was analyzed at least three times in an aqueous environment at 25 °C without further dilution.

The chitosan nanoparticles were viewed with a transmission electron microscope (TEM) (Philips CM12, Andover, MA). 3 ml of 50mM copper sulfate solution was used as a stain solution and added to the particle pellet after centrifugation. The nanoparticles were sonicated to uniformity and soaked in copper sulfate solution for several days under magnetic stirring until equilibrium was reached and then were placed on to imaging grids (Cat. #FCF300-CU from Electron Microscopy Sciences, Hatfield, PA). The grids were subjected to glow discharge treatment before sample loading in order to increase the hydrophilicity of the grid surface.

2.2.4 Microdilution assay

To evaluate the antimicrobial properties of chitosan-based nanoparticles, the samples were tested by performing microdilution assays with several bacterial strains. Each batch of nanoparticles was screened for contamination by plating on Tryptic Soy Agar (TSA) plates. Only sterile samples were used for further assays.

Serial 1:2 dilutions of the antimicrobial treatment were made, then applied to the bacteria being tested at 10^4 cell/well in a 96-well plate. The plate was incubated for 24h, and the wells were examined afterwards for bacterial growth. The lowest concentration of antimicrobial treatment that shows no growth was identified as the Minimal Inhibitory Concentration (MIC), while the next concentration value (2 times that of the MIC) is designated as the Minimal Bacteriocidal Concentration (MBC). Wells from the MIC and MBC concentrations were plated on TSA to confirm non-growth of bacteria for the MBC concentration.

2.3 Results and discussion

2.3.1 Consistency of chitosan nanoparticle properties

During the past two years of work on this project, more than 20 batches of plain chitosan nanoparticles have been synthesized and characterized. Most of the size and zeta potential measurements have been conducted in order to compare with modified chitosan nanoparticles. It is important to point out that we obtained good consistency of the properties of plain chitosan nanoparticles over the past two years. These properties includes not only the size and zeta potential information we obtained from zetasizer measurements (see Table 2-1), but also other parameters such as the yield (~ 0.5 g/ batch), pH of the final suspension (pH 4.5-4.8), and stability, which show the consistency of the particle synthesis operation conducted by multiple people over time. It is well proven that the preparation of chitosan nanoparticles is easy, simple, and well suited for future application in the food industry and other industries which require minimal processing.

Table 2-1 Properties of different batches of chitosan nanoparticles.

Date	size (d.nm)	Pdl	ZP (mV)
4-24-2013*	223.7	0.17	46.5
4-4-2013	254	0.19	52.9
11-30-2012	218.2	0.168	52.5
11-21-2012	236.2	0.162	49.4
9-20-2012	197.8	0.175	47.5

The size and zeta potential of plain chitosan nanoparticles of the marked batch (4-24-2013) are used for comparison to modified chitosan nanoparticles in this work.

To confirm the size and shape of the chitosan nanoparticles, TEM images were obtained (see figure 2-1). Most nanoparticles exhibit a spherical shape without aggregation and their diameters range from 20 nm to 240 nm.

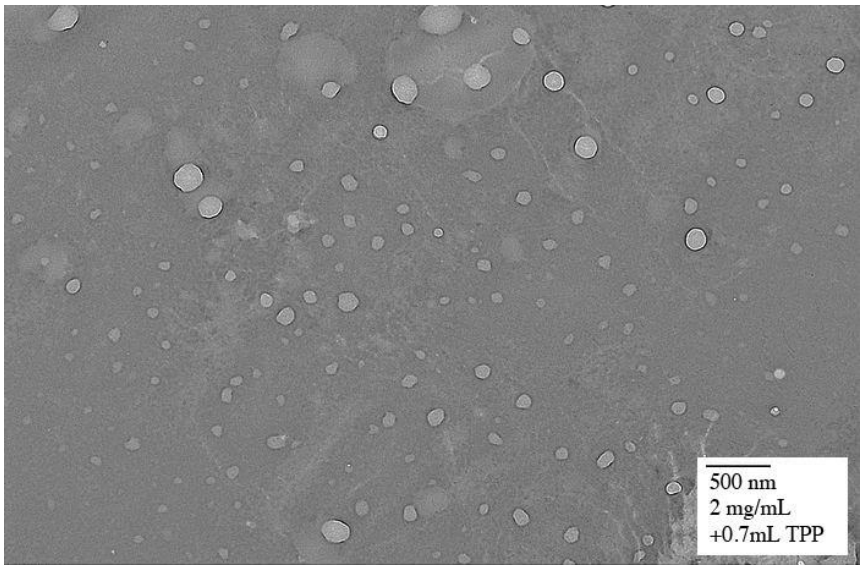

Figure 2-1 TEM image of chitosan nanoparticles prepared with 2 mg/ml chitosan solution and 0.7 ml TPP, stained with copper sulfate solution. Diameter range: approximately 36 – 240 nm. [36]

2.3.2 Attachment of Nisin/ Polylysine

Research regarding particle design focused on the attachment of nisin and polylysine, two antimicrobial peptides widely used as food preservatives, to the surface of chitosan nanoparticles. The surface attachment between antimicrobial peptides and chitosan nanoparticles is formed by ionic bonds or physical absorption due to opposite charge

attraction. The positively charged nanoparticles were soaked in a solution containing oppositely charged tripolyphosphate (TPP) ions or alginate polymer, and then centrifuged and resuspended in a solution containing the antimicrobial peptides. The zeta potential and diameter of the coated nanoparticles were measured in order to optimize the peptide decoration of the chitosan nanoparticles.

Coating with TPP, which is used as the cross-linker in the synthesis of chitosan nanoparticles, tends to reduce the size of the nanoparticles, presumably by forming additional cross-links and thus changing the internal structure of the nanoparticle, not only modifying the surface. A significant amount of nanoparticle aggregation was observed after subsequently attaching either nisin or polylysine.

Alginate coating

Alginate coating lowers the surface charge of chitosan nanoparticles. By increasing the mass ratio of alginate coating to chitosan nanoparticle suspension, the surface charge of the nanoparticles can be decreased to negative values (see table 2-2), which are believed to promote firm attachment between positively charged antimicrobial peptides and chitosan nanoparticles.

Table 2-2 Particle surface charge varies with the mass ratio of chitosan nanoparticle suspension and alginate coating.

mass ratio of chitosan and alginate coating	ZP (mV)
1:0.5	7.66
1:0.7	-4.25
1:1	-15.6
1:1.5	-13.2
1:2	-13.8
1:4	-24.3
1:1 (with nisin coating)	33.7
1:4 (with nisin coating)	31.2

The final mass ratio of chitosan nanoparticle suspension and alginate coating solution used for the following experiments was 1:1. Through the table above, we can see that a greater mass of alginate used for coating can decrease the surface charge of the nanoparticles to more negative values. However, we also want to consider the efficiency of attaching nisin after alginate coating. Comparing the data, we found that the 1:1 mass ratio is enough to have a substantial layer on the surface of chitosan particles. More alginate used may give more negative charge, but after the following steps, it may not work well with another layer of coating. In addition to the change of surface charge after different mass ratios of alginate coating were added, the particle diameter also changed. However, since the alginate coating is an intermediate step of the whole process, there still was excess alginate left to be washed off by following steps, and the samples were not well suited for size measurements.

Nisin coating

Both nisin and polylysine were tested for attachment to alginate-coated chitosan nanoparticles. Results with nisin appear promising. The attachment of nisin brings the nanoparticle surface charge back to positive values. The zeta potential increases along with the diameter of the particles, which indicates that nisin attached on the surface (see table 2-3).

Table 2-3 Particle properties with various mass ratios of nisin coating.

mass ratio of chitosan and nisin coating	ZP (mV)	size (d.nm)
1:0.6	23.7	311
1:1	32.4	588.2
1:2	32.3	655.2
Plain CS NPs	46.5	223.7

Also, washing the particles for one additional time did not significantly change the particles' properties much, which indicates the stability of the peptide attachment (see table 2-4). The approximately doubled average particle size, compared with that of plain chitosan nanoparticles, suggests the presence of mild aggregation.

Table 2-4 Properties of Nisin coated chitosan nanoparticles after additional washing

Sample	ZP (mV)	size (d.nm)
single washed	32.4	588.2
double washed	26.3	565.9

Polylysine incorporation

Due to the strong self-interaction of polylysine coated particles, presumably caused by uneven attachment of the peptides to the nanoparticles, very large particle diameters and relatively low surface charge are observed by zetasizing (see table 2-5).

Table 2-5 Properties of polylysine coated chitosan nanoparticles, compared with nisin coated CS NPs (both of them have a mass ratio of chitosan to polylysine/ nisin of 1:1).

Sample	size (d.nm)	ZP (mV)
Polylysine coated CS NPs	1118	17.4
Nisin coated CS NPs	588.2	32.4

The approach of synthesizing the particles from mixtures of chitosan and polylysine has been tried. Mixtures of chitosan and polylysine of various mass ratios have been prepared. The particles synthesis procedure followed the procedure of preparing chitosan nanoparticles. As the mass ratio of chitosan and polylysine was varied in the initial synthesis solution, changes in surface charge and particle diameter were observed (see table 2-6). It is worth mentioning that the overall polymer concentration is still kept at 2 mg/ml in the mixture of chitosan and polylysine solution. In another words, in these chitosan and polylysine mixed solution, the polylysine solution was substituted for a fraction of the DI water in order to achieve the various mass ratios of chitosan and polylysine in the mixture. In addition, the pH of the chitosan and polylysine mixed solution was maintained at the same value as that of the plain chitosan synthesis solution by replacing small amounts of DI water with acetic acid.

Table 2-6 Properties of polylysine incorporated chitosan nanoparticles.

mass ratio of chitosan and polylysine	size (nm)	ZP (mV)
5:1	206.1	44.5
10:1	206.5	46.9
20:1	233.6	47.3
Plain CS NPs	223.7	46.5

The polylysine incorporated chitosan nanoparticles still exhibit high positive surface charge, which is very promising for antimicrobial properties and interaction with gram-negative bacteria. The mass ratio of chitosan and polylysine was kept at 10:1 for further sample preparation due to its relatively high surface charge and small particle diameter.

2.3.3 Microdilution assay

A number of antimicrobial agents with demonstrated antibacterial efficacy are screened in the microdilution assay in order to identify the level of antimicrobial activity against the strains of bacteria used in chitosan nanoparticle tests (see Table 2-7). The substances used in the assays are chosen due to their GRAS status and/or their application in food production, as this project is aiming to develop chitosan-based polymeric nanoparticles to use in a food-processing environment. Differences in antimicrobial activity are apparent for gram positive and gram negative bacteria, as well as among contrasting strains of the same type.

Table 2-7 MIC for antimicrobial agents against several bacteria strains.

Bacterial strain	nisin (μg/ml)	ε-poly-L-lysine (μg/ml)	EDDS (w/v %)	lauric arginate (μg/ml)	zinc lactate (μg/ml)
Escherichia coli O157:H7 ATCC#43895	>2000	156	9 %	78	2500
Escherichia coli O157:H7 ATCC#06024	>2000	156	9 %	78	5000
Listeria monocytogenes J1-110	625	5	1 %	78	1250
Staphylococcus aureus ATCC#10832	156	50	2 %	39	2500
Staphylococcus aureus ATCC#25923	156	50	2 %	39	1250

Plain chitosan nanoparticles (CS NPs) were used in microdilution assay to test the antimicrobial activity against several strains of bacteria (see Table 2-8).

Table 2-8 MIC for chitosan-based nanoparticles against different strains of bacteria.

Bacterial strain	Gram	MIC
Escherichia coli O157:H7 ATCC#43895	-	> 2mg/ml
Escherichia coli O157:H7 ATCC#06024	-	> 2mg/ml
Listeria monocytogenes J1-110	+	4 μg/ml
Staphylococcus aureus ATCC#10832	+	> 2mg/ml
Staphylococcus aureus ATCC#25923	+	> 2mg/ml
Salmonella agora	-	> 2mg/ml
Salmonella montevideo	-	> 2mg/ml
Bacillus cereus	+	> 2mg/ml

Comparing Table 2-7 and 2-8, we can see that the minimal concentration of chitosan nanoparticles needed to inhibit microbial growth is relatively high (in the milligram range based on the wet mass) compared with most antimicrobial substances tested. Note that for a direct comparison to the other antimicrobial substances, the dry mass of nanoparticles must be used, which is lower than the wet mass by a factor of 18.44 [36]. Applying the chitosan nanoparticles suspension at such a high concentration for industrial use would be non-cost-efficient, and may potentially cause visual or textural changes in the commodities being targeted. To address this problem, the combination of an effective antimicrobial substance with the chitosan nanoparticles would be able to lower the effective concentration of chitosan nanoparticles. Besides elucidating the MIC of the chitosan nanoparticles and the screening of various antimicrobial chemicals, these preliminary experiments have been conducted on multiple species of bacteria to select one or two suitable species for more focused test of antimicrobial combined chitosan nanoparticles in the future.

2.4 Summary

Plain chitosan nanoparticles synthesized with an optimal concentration of TPP solution were investigated for attachment of antimicrobial peptides on the surface or incorporation during the synthesis process. Alginate, as a bonding layer between two cationic species, chitosan and nisin, shows stable interactions with both of them through electrostatic forces. For polylysine, a different method was used to incorporate it inside of the chitosan nanoparticles. Various mass ratios of chitosan and polylysine in the nanoparticle synthesis solution have been investigated, and the ratio of 10:1 was used in the following experiments. This novel chitosan-based nanoparticles is successfully decorated with antimicrobials using different attaching methods.

Chitosan was realized in nanoparticles form for food application use. And the potential synergistic effect of the antimicrobial properties of chitosan and antimicrobial peptide on both Gram positive and Gram negative bacteria are expected. Plain chitosan nanoparticles, nisin coated chitosan nanoparticles, and polylysine incorporated chitosan nanoparticles were prepared for further investigation of antimicrobial effectiveness.

Chapter 3 Synthesis and characterization of conjugated polymer-based luminescent oxygen-sensitive nanoparticles

3.1 Introduction

Oxygen is one of the most important chemical species on the earth, especially for human beings. Quantitative determination of oxygen content, both in gas[16] and liquid phase[17], is of great importance for various fields, for example medicine, biology, food manufacturing, oceanography, environmental monitoring, etc.[18]. Based on different measuring methods, oxygen sensors can be divided into three categories: electrochemical[19], optical[20-22], and chemical (Winkler titration[23]).

Optical oxygen sensor received great attention recently due to its advantages over other methods: inexpensive, easily miniaturized, simple preparation, no electrical interference, and not oxygen consuming[20]. The major principle used for optical oxygen sensor is the quenching of the luminescence of an indicator dye by molecular oxygen[24]. The typical layout for an optical oxygen sensor consists of a luminescent indicator dye immobilized in a polymeric matrix, and deposited on a solid support (planar waveguide, microtitre plate, or optical fiber)[25].

The application area is also a critical factor for the design of optical oxygen sensors. In recent years, a great attention has been focused on the understanding of cellular function and processes taking place in both normal and abnormal cells and tissues[26]. In biological system, oxygen, as a small gaseous analyte, diffuses fast in solution, in and out of the cell, and is present in vast excess in the environment[27]. Therefore, it raises the

demand the development of an accurate oxygen sensor which is versatile, flexible and simple. To satisfy these requirement, the “perfect” sensor should have high brightness, ability for cell penetration, be suitable for ratiometric two-wavelength measurement, potential for two-photon absorption, simple preparation and low working concentrations. Several kinds of particle based cellular/ intracellular oxygen sensors have been presented by scientists [27-32], which met some of the requirement.

In this work, we present a series of conjugated polymer-based oxygen-sensitive nanoparticles, with high brightness, under dual emission for ratiometric measurement, functional groups for water dispersibility and cell penetration.

3.2 Experimental methods

3.2.1 Materials

All the used chemicals are listed in Table 3-1.

Table 3-1 Used chemicals.

Chemical	**Supplier**	**CAS number**
Acetone	Brenntag	76-64-1
Dichloromethane	VWR	75-09-2
Dichloromethan anhydrous	Sigma-Aldrich	75-09-2
N,N-Dimethylformamid anhydrous	Sigma-Aldrich	68-12-2
Ethylacetate	VWR	141-78-6
Ethanol	Brenntag	64-17-5
Tetrahydrofuran	VWR	109-99-9
Toluene	VWR	108-88-3
1,2,4-Trimethylbenzene	Sigma-Aldrich	95-63-6
Silica Gel	Acros	112926-00-8
Tetrakis(triphenylphosphin)palladium	ABCR	14221-01-3
K_2CO_3	Roth	584-08-7
Methanol	Roth	67-56-1
Sodium hydroxide (0.1 M)	Roth	1310-73-2
Sodium sulphate	VWR	7757-82-6
Sodium chloride	Fluka	7647-14-5
9,9-Diheptylfluorene-2,7-diboronic acid	Frontier	916336-19-1
4-(tert-Butyl)phenylboronic acid	Frontier	123324-71-0
[9,9-Di(p -tolyl)-fluoren-2,7-diyl]diboronic acid	Lumtec	
2,7-Dibromo-9,9-di-p -tolyl-9H -fluorene	Lumtec	357645-37-5
4,7-Bis(5-bromothiophen-2-yl) benzo[c][1,2,5]thiadiazole	Lumtec	288071-87-4

3,3'-(2,7-Dibromo-9H-fluorene-9,9-diyl)bis(N,N-dimethylpropan-1-amine)	Lumtec	673474-73-2
4,7-Dibromobenzo[c]-1,2,5-thiadiazole	Sigma-Aldrich	15155-41-6
Bis(di-tert-butyl(4-dimethylaminophenyl)phosphine)dichloropalladium(II)	Acros	887919-35-9
1,5-Diiodopentane	ABS	628-77-3
1-Bromo-2-(2-methoxyethoxy)ethane	ABS	54149-17-6
Tetrabutylammonium bromide	Sigma-Aldrich	1643-19-2
2,7-Dibromofluorene	Sigma-Aldrich	16433-88-8
$H_2TPTBPtBu_4Br_4$	synthesized at TU Graz	
Pt(II)–5,15-di(pentafluorophenyl)-10,20-di(4-bromophenyl)porphyrin (PtTFPP)	synthesized at TU Graz	

3.2.2 Monomer synthesis

Anionic monomer – Dimethyl 3,3'-(2,7-dibromo-9H-fluorene-9,9-diyl)dipropanoate [101]

2,7-Dibromofluorene (500 mg, 1.55 mmol), methyl acrylate (430.5 mg, 5 mmol) tetrabutylammonium bromide (50 mg, 0.15 mmol) and toluene (2.5 ml) were added to a small round bottom flask with a Teflon-coated stirbar. Next 1 ml of 50% NaOH (aq) was added while stirring. The reaction was allowed to proceed overnight at room temperature. The next day the toluene layer was transferred to a flask and the aqueous layer was extracted with two portions of toluene. The organic layers are combined, dried with Mg_2SO_4, and filtered. Silica (2 g) was added to the filtrate and the solution was evaporated under N_2. The product was purified via column chromatography on silica gel packed with cyclohexane. Impurities were washed out by toluene and the clean product

was eluted with a mixture of toluene and ethyl acetate (1:1). After drying in vacuum oven overnight, the pure product was obtained as a white solid. Yield 2.09 g. ^{1}H NMR (300 MHz, $CDCl_3$) δ, ppm: 7.55-7.46, m, 6H, Ar; 3.49, s, 6H, -$COOCH_3$; 2.37, t, 4H, CH_2-$\underline{CH_2}$-$COOCH_3$; 1.57, t, 4H, $\underline{CH_2}$-CH_2-$COOCH_3$. Figure 4.1 Shows ^{1}H and COSY NMR spectra of the compound.

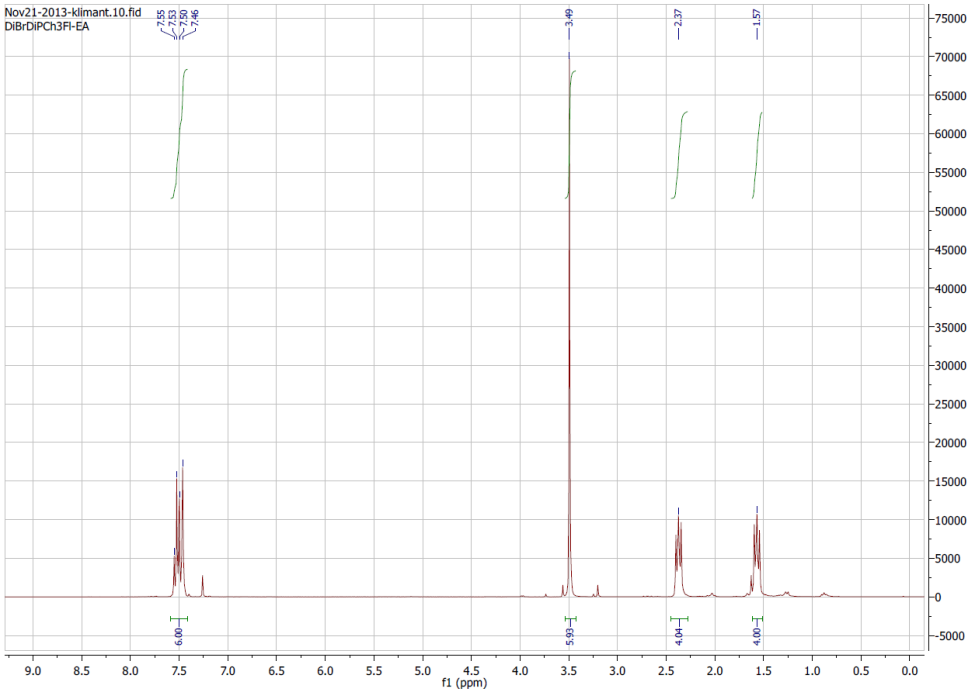

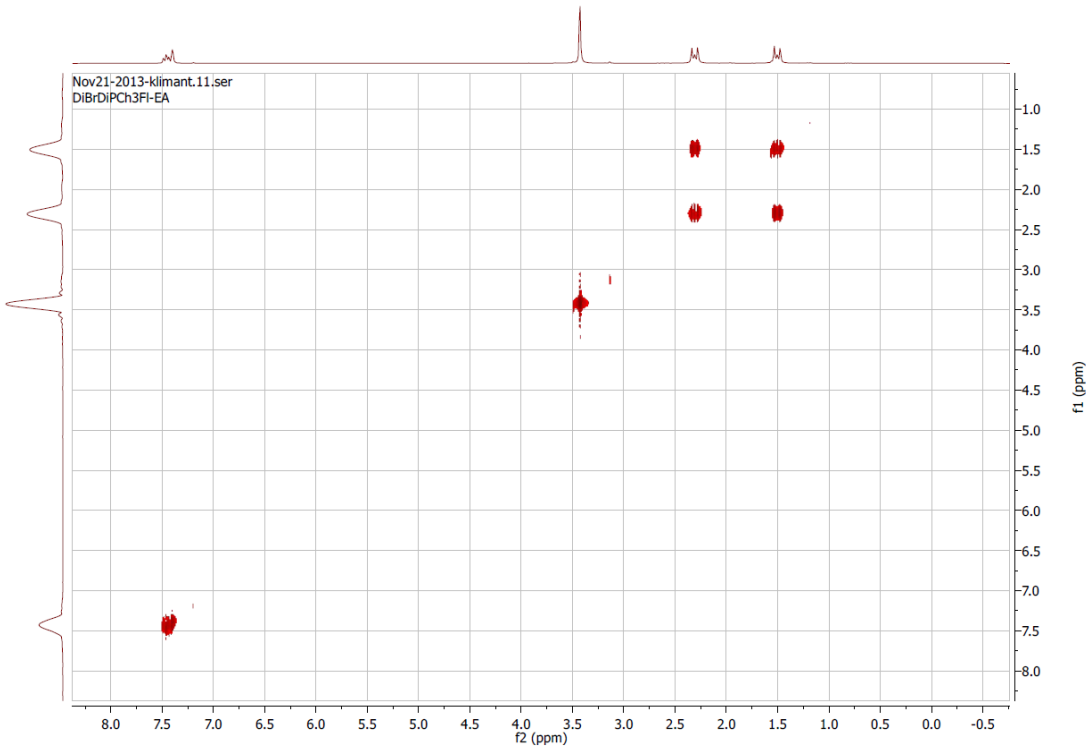

Figure 3-1 ^{1}H and COSY NMR spectra of the dimethyl 3,3'-(2,7-dibromo-9H-fluorene-9,9-diyl)dipropanoate.

3.2.3 Dye synthesis (PtTPPtBuBP)

Platinum (II) meso-tetra(4-bromophenyl)tetra(*tert-butyl*)benzoporphyrin

$H_2TPTBPtBu_4Br_4$ (500 mg, 0.369 mmol) was dissolved in 250 ml trimethylebenzene and heated to 155 ℃ in a 2-neck round bottle. N_2 was bubbled through the reaction mixture and $Pt(BN)_2Cl_2$ (260 mg, 0.554 mmol) was added in small pre-dissolved portions over 4 hours. The reaction was monitored via UV-Vis spectroscopy. The solvent was removed using a rotary evaporator at 70 ℃ and the crude product was purified using column chromatography (Al_2O_3, Cyclohexene/Dichloromethane 5/1). The solvent was removed and the product was placed in a 2-neck round-bottle with cold finger. The viscous

product was heated to 350 ℃ under high vacuum to remove side products (Yield 404 mg, 0.263 mmol, 71%).

3.2.4 Conjugated polymers synthesis

The conjugated polymers were prepared through Suzuki coupling between various platinum (Ⅱ) porphyrin complexes and one to one ratio of diboronic acid and dibromo derivatives as building blocks. Different dibromo derivatives were used to give different functions to the conjugated polymers. For example, 4,7-bis(5-bromothiophen-2-yl)benzo[c][1,2,5]thiadiazoles shifts the excitation and emission wavelength of conjugated polymers to near-infrared(NIR) wavelength.

3.2.4.1 PtTFPP integrated cationic conjugated polymer

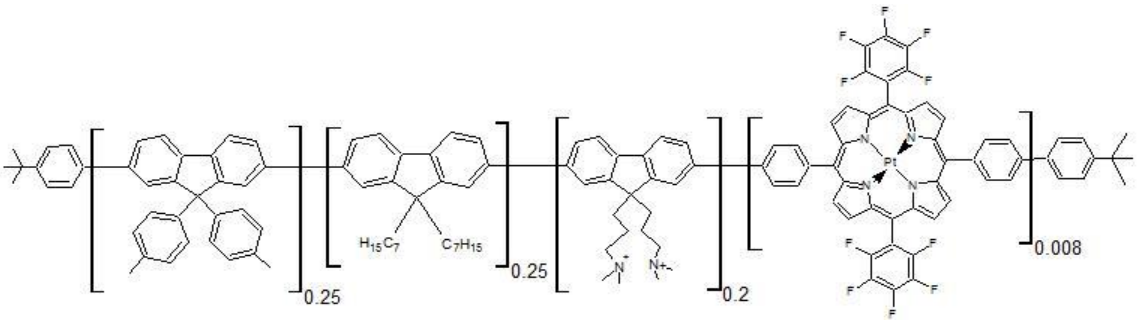

Figure 3-2 Structure of PtTFPP integrated cationic conjugated polymer

[9,9-di-p-tolyl-fluoren-2,7-diyl]diboronic acid (110.7 mg, 0.25 mmol), 9,9-diheptylfluorene-2,7-diboronic acid (114.8 mg, 0.25 mmol), 2,7-dibromo-9,9-di-p-tolyl-9H-fluorene (154.4 mg, 0.3 mmol), 3,3'-(2,7-dibromo-9H-fluorene-9,9-diyl)bis(N,N-dimethylpropan-1-amine) (100.9 mg, 0.2 mmol), and Pt(II)–5,15-di(pentafluorophenyl)-10,20-di(4-bromophenyl)porphyrin (PtTFPP) (9 mg, mmmol) were dissolved in the

mixture of 5 ml toluene and 1.7 ml tetrahydrofuran in Schlenk flask with a Teflon-coated stir bar. Next, potassium carbonate (276 mg, 2 mmol) dissolved in 1.5 ml deionized (DI) water and bis(di-tert-butyl(4-dimethylaminophenyl)phosphine)dichloropalladium(II) (10.4mg, 3mol%) dissolved in 1 ml toluene were added into Schlenk flask while stirring. The reaction was allowed to proceed overnight at 80 °C. The next day, 2,7-dibromo-9,9-di-p-tolyl-9H-fluorene (10.3 mg, 0.02 mmol) and 4-tert-butylphenylboronic acid (8.9 mg, 0.05mmol) were added into reaction with 1.5 hours in between. After another 1.5 hour the flask was left at room temperature to cool down. The organic layer was transferred to a flask and the aqueous layer was extracted with two portions of dichloromethane. The organic layers are combined, dried with Mg_2SO_4, and filtered, if necessary. Then organic phase was added dropwise into 6 times volume of methanol to precipitate the product. After filtering, the sediments were dried on filter paper in oven at 60 °C overnight. The polymer was obtained as a red solid (225.3 mg, 66.0% yield).

The polymer was rendered cationic via alkylation. 50 mg of the polymer, 2.5 ml of toluene, 24.2 mg (0.2 mmol) of potassium carbonate and 14mg (0.1 mmol) of methyl iodide were added into Schlenk flask with a Teflon-coated stirbar. The reaction was done at 80 °C under argon gas for 4 hours. The organic layer was transferred to a flask. After distillation at reduced pressure, the PtTFPP integrated cationic conjugated polymer was dissolved in acetone and THF mixture as “cocktail” to make particles.

3.2.4.2 PtTFPP integrated anionic conjugated polymer

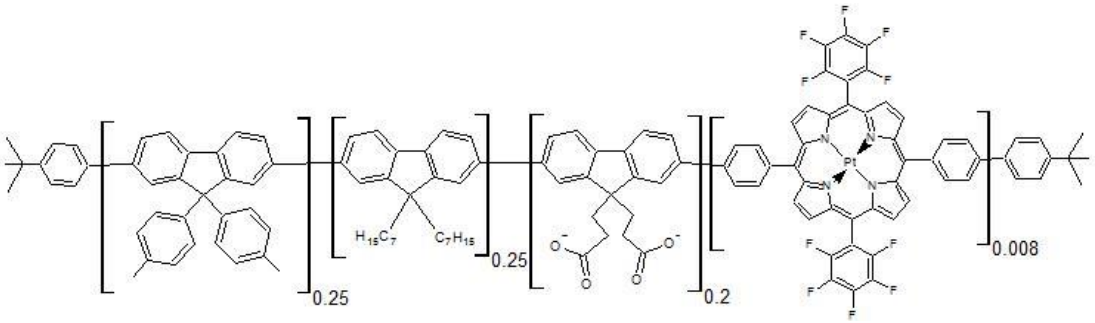

Figure 3-3 Structure of PtTFPP integrated anionic conjugated polymer

[9,9-di-p-tolyl-fluoren-2,7-diyl]diboronic acid (110.7 mg, 0.25 mmol), 9,9-diheptylfluorene-2,7-diboronic acid (114.8 mg, 0.25 mmol), 2,7-dibromo-9,9-di-p-tolyl-9H-fluorene (154.4 mg, 0.3 mmol), dimethyl 3,3'-(2,7-dibromo-9H-fluorene-9,9-diyl)dipropanoate (101.3 mg, 0.2 mmol), and PtTFPP (9 mg) were dissolved in 5 ml toluene and 1.7 ml tetrahydrofuran (THF) mixture in Schlenk flask with a Teflon-coated stir bar. Next, potassium carbonate (276 mg, 2 mmol) dissolved in 1.5 ml deionized (DI) water and bis(di-tert-butyl(4-dimethylaminophenyl)phosphine)dichloropalladium(II) (10.4mg, 3mol%) dissolved in 1 ml toluene were added into Schlenk flask while stirring. The reaction was allowed to proceed over night at 80 °C. The next day, 2,7-dibromo-9,9-di-p-tolyl-9H-fluorene (10.3 mg, 0.02 mmol) and 4-tert-butylphenylboronic acid (8.9 mg, 0.05mmol) were added into reaction with 1.5 hours in between. After another 1.5 hour, the reaction was done and left at room temperature to cool down. The organic layer was transferred to a flask and the aqueous layer was extracted with two portions of dichloromethane. The organic layers are combined, dried with Mg_2SO_4, and filtered, if necessary. Then organic phase was added dropwise into 6 times volume of methanol to

precipitate the product. After filtering, the sediments were dried on filter paper in oven at 60 °C overnight. The polymer was obtained as a red solid (237.2 mg, 85.4% yield).

The polymer was rendered anionic via hydrolysis. 50 mg of the polymer, 5 ml of THF, and 100 μl of 1M NaOH were added into a flask with a Teflon-coated stir bar. The reaction was done at 40 °C for 1 hour. The PtTFPP integrated anionic conjugated polymer was dissolved in additional 7.5 ml THF and 12.5 ml acetone solution as "cocktail" to make particles.

3.2.4.3 PtTFPP integrated "zwitterionic" conjugated polymer

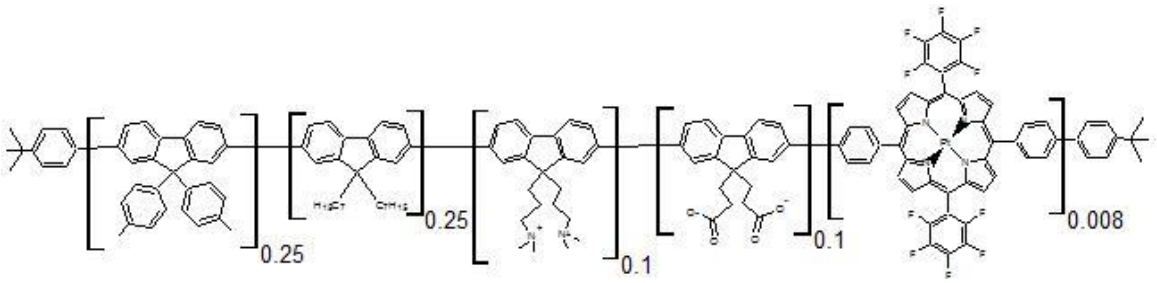

Figure 3-4 Structure of PtTFPP integrated zwittertionic conjugated polymer

The basic procedure of Suzuki coupling is similar as PtTFPP integrated cationic/ anionic conjugated polymers, except we have both cationic and anionic monomers inside. The following components were used: [9,9-di-p-tolyl-fluoren-2,7-diyl]diboronic acid (110.7 mg, 0.25 mmol), 9,9-Diheptylfluorene-2,7-diboronic acid (114.8 mg, 0.25 mmol), 2,7-dibromo-9,9-di-p-tolyl-9H-fluorene (154.4 mg, 0.3 mmol), 3,3'-(2,7-dibromo-9H-fluorene-9,9-diyl)bis(N,N-dimethylpropan-1-amine) (100.9 mg, 0.2 mmol), dimethyl 3,3'-(2,7-dibromo-9H-fluorene-9,9-diyl)dipropanoate (101.3 mg, 0.2 mmol), and PtTFPP (9 mg).

To have both cationic and anionic monomers to be functionalized, both alkylation and hydrolysis have been done, in the same order. The “cocktail” of the polymers in 25 ml THF and acetone mixture was obtained to make particles.

3.2.4.4 PtTPTtBuBP integrated cationic conjugated polymer

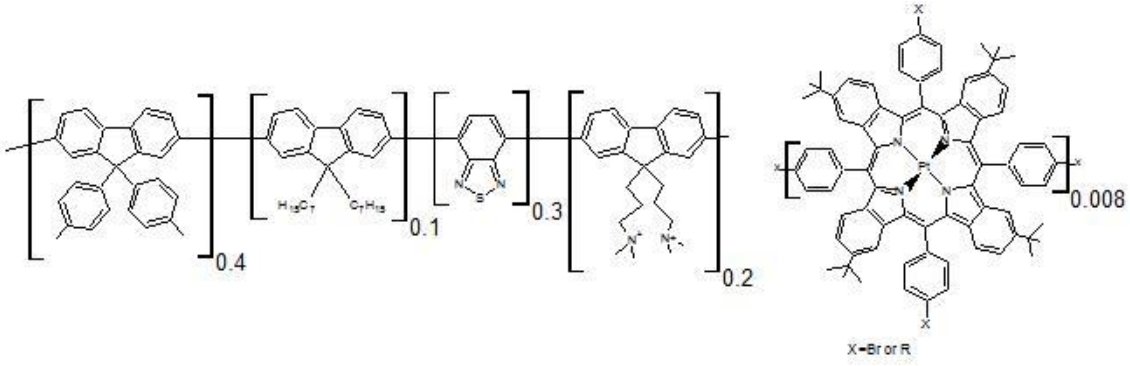

Figure 3-5 Structure of PtTPTtBuBP integrated cationic conjugated polymer

[9,9-di-p-tolyl-fluoren-2,7-diyl]diboronic acid (177.2 mg, 0.4 mmol), 9,9-diheptylfluorene-2,7-diboronic acid (45.9 mg, 0.1 mmol), 4,7-dibromobenzo[c]-1,2,5-thiadiazole (89.9 mg, 0.3mmol), 3,3'-(2,7-dibromo-9H-fluorene-9,9-diyl)bis(N,N-dimethylpropan-1-amine) (100.9 mg, 0.2mmol), and PtTPTBTPF (7 mg) were dissolved in 5 ml toluene and 1.7 ml THF mixture in Schlenk flask with a Teflon-coated stir bar. Next, potassium carbonate (276 mg, 2 mmol) dissolved in 1.5 ml deionized (DI) water and bis(di-tert-butyl(4 dimethylaminophenyl)phosphine)dichloropalladium(II) (10.4mg, 3mol%) dissolved in 1 ml toluene were added into Schlenk flask while stirring. The reaction was allowed to proceed overnight at 80 °C. The next day, 4,7-dibromobenzo[c]-1,2,5-thiadiazole (5.99 mg, 0.02 mmol) and 4-tert-butylphenylboronic acid (8.9 mg, 0.05mmol) were added into reaction with 1.5 hours in between. After another 1.5 hour,

the reaction was done and left at room temperature to cool down. The following procedures are same as PtTFPP-integrated cationic conjugated polymers. A green solid was obtained as product. (114.0 mg, 53.8% yield).

To render the polymer cationic, the alkylation was performed using the procedure established for PtTFPP-modified polymers

3.2.4.5 PtTPTtBuBP integrated anionic conjugated polymer

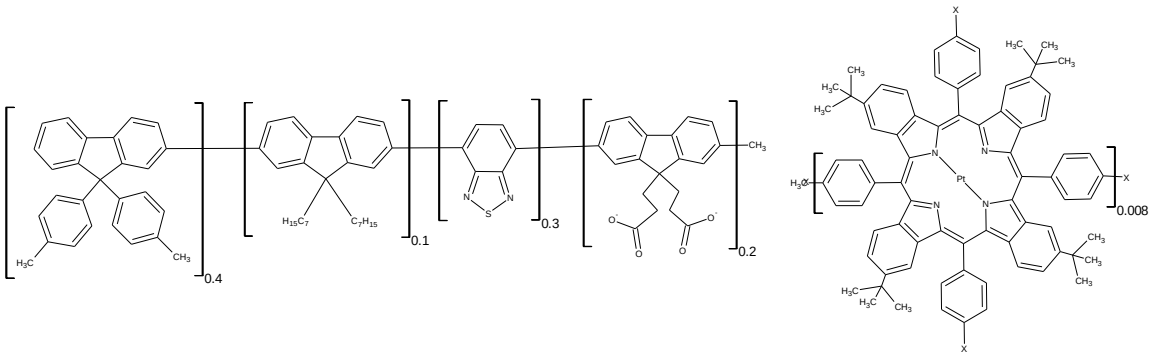

Figure 3-6 Structure of PtTPTtBuBP integrated anionic conjugated polymer

[9,9-di-p-tolyl-fluoren-2,7-diyl]diboronic acid (177.2 mg, 0.4 mmol), 9,9-diheptylfluorene-2,7-diboronic acid (45.9 mg, 0.1 mmol), 4,7-dibromobenzo[c]-1,2,5-thiadiazole (89.9 mg, 0.3mmol), dimethyl 3,3’-(2,7-dibromo-9H-fluorene-9,9-diyl)dipropanoate (101.3 mg, 0.2 mmol), and PtTPTtBuBP (3.5 mg) were dissolved in 5 ml toluene and 1.7 ml THF mixture in Schlenk flask with a Teflon-coated stir bar. Next, potassium carbonate (276 mg, 2 mmol) dissolved in 1.5 ml deionized (DI) water and Bis(di-tert-butyl(4-dimethylaminophenyl)phosphine)dichloropalladium(II) (10.4mg, 3mol%) dissolved in 1 ml toluene were added into Schlenk flask while stirring. The reaction was allowed to proceed over night at 80 °C. The next day, 4,7-Dibromobenzo[c]-

1,2,5-thiadiazole (5.99 mg, 0.02 mmol) and 4-tert-Butylphenylboronic acid (8.9 mg, 0.05mmol) were added into reaction with 1.5 hours in between. After another 1.5 hour, the reaction was done and left at room temperature to cool down. The procedure used for the PtTFPP-integrated anionic conjugated polymers was used. A green solid was obtained as product. (86.0 mg, 42.0 % yield).

To have the anionic function, hydrolysis was done the next day, which is exactly the same as alkylation for PtTFPP integrated anionic conjugated polymers.

3.2.5 Preparation of conjugated polymer-based nanoparticles

First, 50 mg of the conjugated polymer were dissolved in 30 ml of acetone : THF mixture. The solution was transfered into 150 ml glass beaker equipped with a teflon-coated stir bar.. Then, 125 ml of DI water was added to the stirred solution (400 rpm) within 3 seconds. A transparent colored dispersion of the nanoparticles was formed. The dispersion of the nanoparticles was placed in 250 ml round flask and acetone and THF and partly water were removed reduced pressure (by gradually reducing pressure up to about 80 mbar). The dispersion was concentrated to about 35 ml and was stored in screw cap vials at 4 ℃.

3.2.6 Photophysical measurements

Absorption

Absorption measurements were performed between 800nm and 350nm on a "Varian Cary 50 Conc "UV-Vis spectrophotometer by Varian, Palo Alto, United States

(www.varianinc.com), set at a fast scan rate using baseline correction and an adequate blank sample. Hellma 100-QS 10mm precision cuvettes or Hellma 101-OS 10mm precision cuvettes were used. Molar absorption coefficients were calculated using Lambert-Beers law.

Emission and Excitation Spectra

Emission and excitation spectra were recorded on a Hitachi-F-7000 spectrofluorometer in Hellma 101-OS 10mm precision cuvettes or Hellma screw-cap fluorescence cuvettes and corrected for detector response.

Single Photon Counting

The fluorescence decay times were acquired using single photon counting technique on a FluoroLog Spectrofluorometer from Horiba Scientific equipped with a DeltaHub module. Data were fitted using a mono-exponential fit or bi-exponential fit.

3.2.7 Structural and chemical measurements

^{1}H NMR

^{1}H NMR spectra were recorded on a 300MHz Bruker instrument (www.bruker.com). The analysis of the data was conducted with MNova NMR software (www.mestrelab.com).

Size and Zeta-potential

The size of the beads and Zeta potential were determined with a particle size analyzer Zetasizer Nano ZS (www.malvern.de).

3.3 Results and discussion

The aim of this work is the development of conjugated polymer-based oxygen sensitive nanoparticles, with high brightness, under dual emission for ratiometric measurements, functional groups for water dispersibility and cell penetration.

The scientific strategy to obtain this kind of oxygen sensitive nanoparticles was to co-polymerize oxygen indicator, additional functional groups, e.g. the charged group, inside of the conjugated polymers.

3.3.1 Synthetic considerations

Suzuki coupling is an established way to produce conjugated polymers. It is modular, different blocks (dibromo- and diboronic acid derivatives) can be combined in an alternating polymer. Functionalities can be incorporated. Better use neutral functionalities and render them charged already in the polymer. Neutral polymer is easier to obtain, no redistribution of the monomers between organic and aqueous phases, easier purification of the uncharged polymer from oligomers. Other dyes can be incorporated as well (such as porphyrins used here). Dibromo derivatives are preferable; however 4 Br derivatives (see Pt-bennzoporphyrins) may be used in small concentration (which is high enough for the applications). The risk of cross-linking is small at these concentrations.

3.3.2 Brightness of conjugated polymer-based oxygen-sensitive nanoparticles

3.3.2.1 PtTFPP integrated conjugated polymer-based oxygen-sensitive nanoparticles

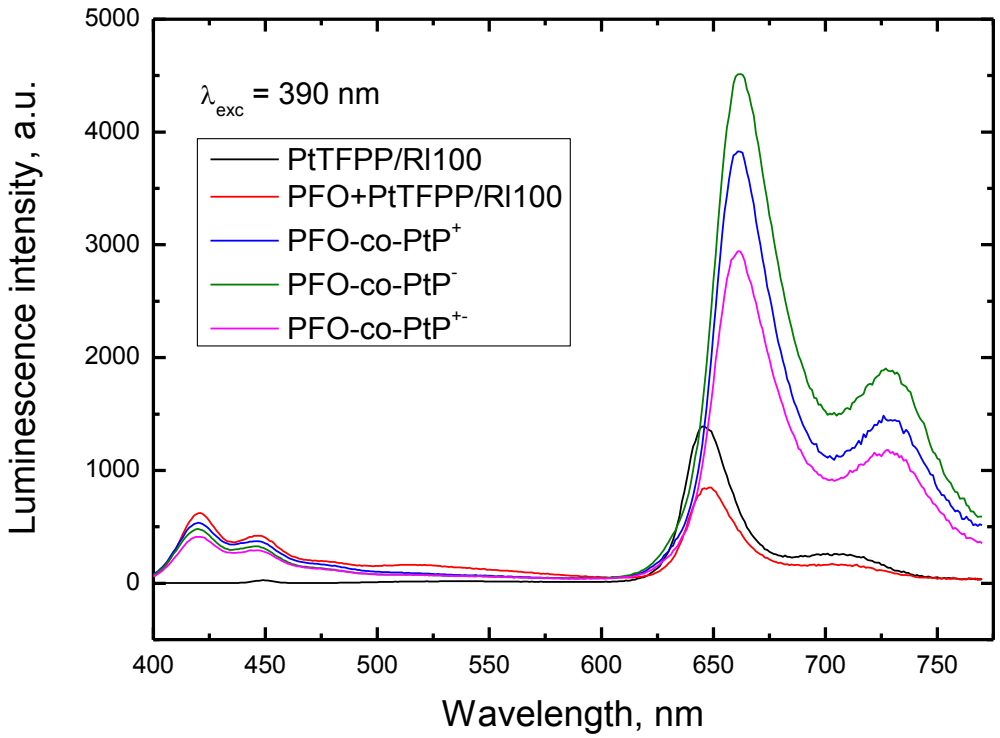

Figure 3-7 Corrected Emission spectra of PtTFPP integrated conjugated polymer-based oxygen sensitive nanoparticles (λ_{exc} = 390 nm, identical absorption of all samples at this wavelength)

The brightness of three kinds of PtTFPP integrated conjugated polymer-based oxygen-sensitive nanoparticles we prepared has been compared with two other kinds of oxygen-sensitive nanoparticles we worked on before. PtTFPP-RL-100 nanoparticles have 1.5% w/w dye incorporated in highly positively charged Eudragit RL-100 polymer by means of

physical inclusion[27]. Another oxygen nanosensor PFO-PtTFPP-RL-100 has the hydrophobic conjugated polyfluorene PFO (acting an energy donor) incorporated along with the oxygen indicator PtTFPP (acting as an energy acceptor) in RL-100[31]. It also allows for ratiometric or multiphoton imaging of oxygen. Both of these kinds of oxygen sensitive nanosensors show good brightness.

Comparing emission spectra of these oxygen nanosensors with 390 nm wavelength excitation, a significant improvement of brightness has been achieved by the synthesis of PtTFPP integrated conjugated polymer-based oxygen sensitive nanoparticles. Brightness of the.cationic, anionic and zwitterionic polymeric particles is similar. It is around 6 times and 4 times brighter than PtTFPP-RL-100 and PFO-PtTFPP-RL-100 nanoparticles, respectively. Similarly to the PFO-PtTFPP-RL-100 particles, the new polymeric beads allow for ratiometric measurement of oxygen due to the emission in both blue and red part of the spectrum.

It is interesting to note that the emission wavelength of PtTFPP in conjugated polymer-based nanoparticles is slightly shifted (about 15 nm) to longer wavelength. This is likely to be caused by increased pi-conjugation of the porphyrin incorporated into the conjugated polymer.

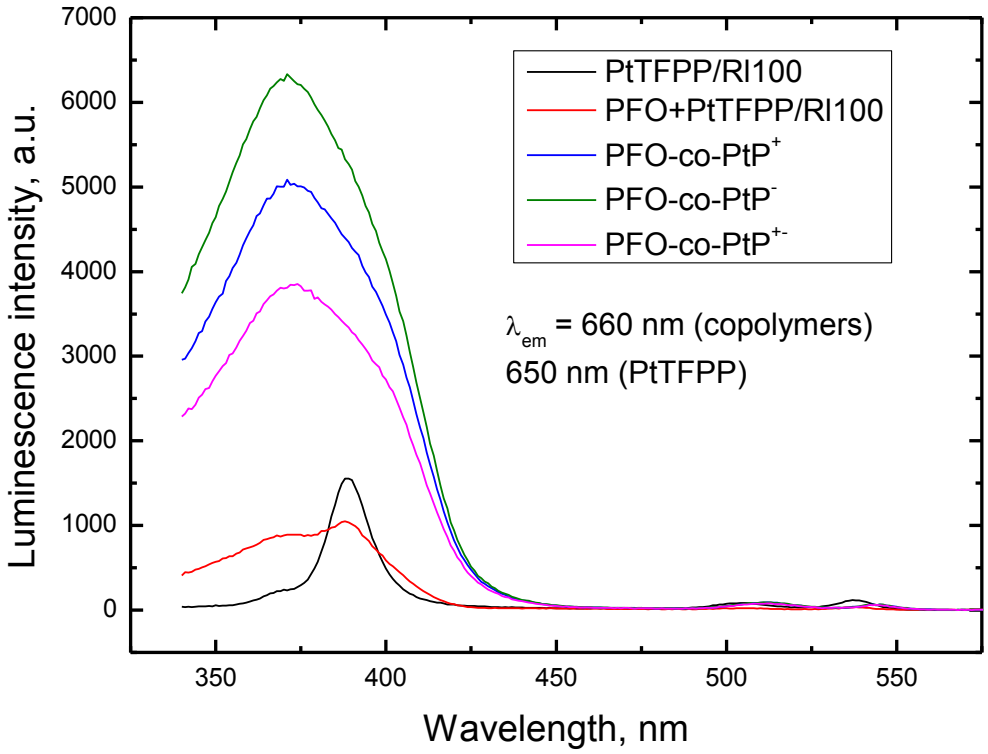

Figure 3-8 Excitation spectra of PtTFPP integrated conjugated polymer-based oxygen sensitive nanoparticles. (λ_{em} = 660 nm, conjugated polymers; λ_{em} = 650 nm PtTFPP)

Excitation spectra of PtTFPP integrated conjugated polymer-based oxygen sensitive nanoparticles indicates that the energy transfer from conjugated polymers to oxygen indicator (PtTFPP) is very efficient. Indeed, the excitation arises from the conjugated polymer, and only very small bans corresponding to the direct excitation of PtTFPP (510 and 540 nm) are visible.

We also noticed that, at the maxima emission wavelength of PtTFPP (650 nm in RL-100 polymer matrix, 660 nm in conjugated polymer matrix), excitation via conjugated

polymer in conjugated polymer matrix is 5 – 6 times higher than in RL-100 polymer matrix . So we are able to say the energy transfer in conjugated polymer is significantly efficient in our conjugated polymer-based oxygen sensitive nanoparticles.

3.3.2.2 PtTPTtBuBP integrated conjugated polymer-based oxygen-sensitive nanoparticles

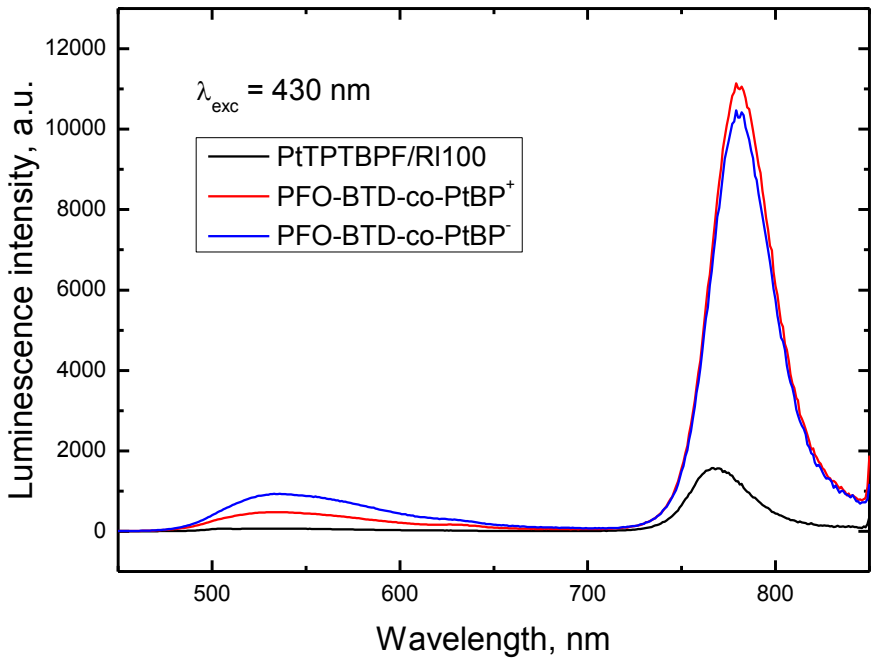

Figure 3-9 Corrected Emission spectra of PtTPTtBuBP integrated conjugated polymer-based oxygen sensitive nanoparticles (PFO-BTD-co-PtBP) and PtTPTBPF-doped Rl-100 nanoparticles used for comparison (λexc = 430 nm, the absorption at this wavelength is kept constant for all the materials))

Two kinds of PtTPTtBuBP integrated conjugated polymer-based sensitive nanoparticles have been prepared. One is positively charged and the other is negatively charged.

Compared toPtTPTBPF incorporated RL-100 nanosensor, a factor of 6 of brightness enhancement has been achieved by conjugated polymer-based nanosensor. Importantly, the green emission originating from the conjugated polymer can again be used for the ratiometric referencing.

The maxima emission wavelength of PtTPTBPF is around 780 nm. This near-infrared emission spectra is more preferred, since it reduced the noise of autofluorescence in biological system. Again, conjugation may slightly affect the emission of the porphyrin in the conjugated polymer (a bathochromic shift of 10 nm compared to the PtTPTBPF-based particles). However, the electron-donating t-Bu groups of the porphyrin may also be responsible for this effect.

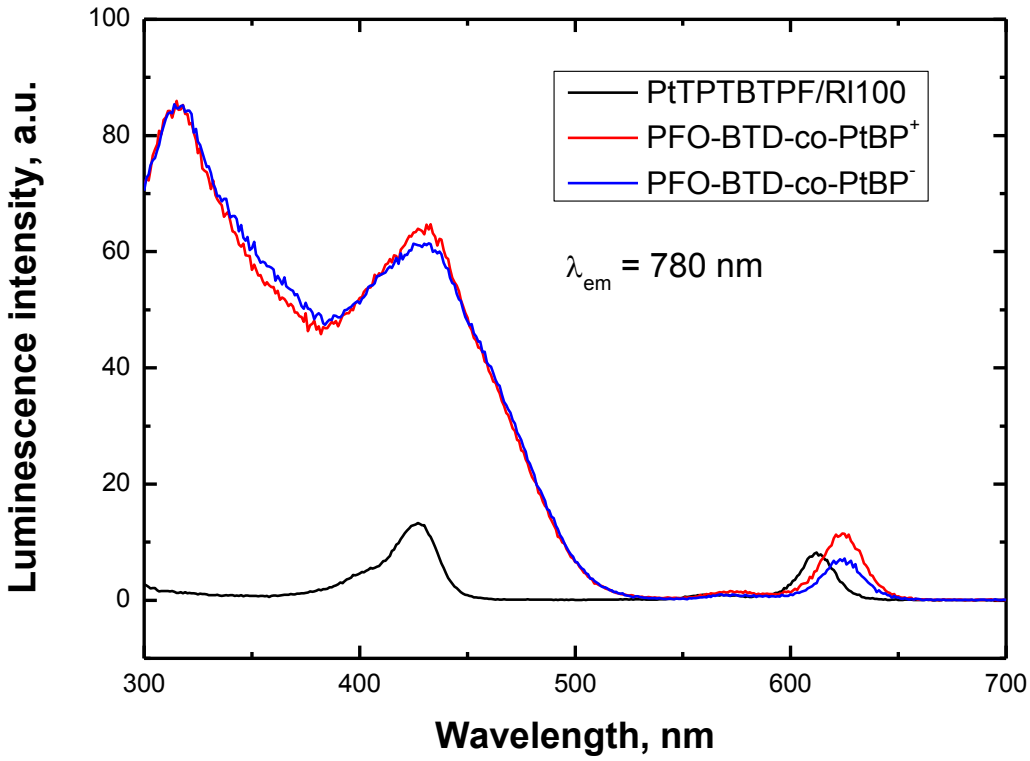

Figure 3-10 Excitation spectra of PtTPTtBuBP integrated conjugated polymer-based oxygen-sensitive nanoparticles and PtTPTBPF-doped Rl-100 nanoparticles used as a reference. (λ_{em} = 780 nm)

An efficient energy transfer from the conjugated polymer to PtTPTtBuBP in conjugated polymer-based nanoparticles is evident (Figure 5.4.). Corresponding to the emission spectra, enhancement by the factor of 6 or more is established in both cationic and anionic conjugated polymer-based oxygen sensitive nanoparticles, compared with PtTPTBPF incorporated RL-100 polymer-based oxygen sensitive nanoparticles.

3.3.3 Energy transfer in the conjugated polymer-based oxygen-sensitive nanoparticles

As was described above, the efficient energy transfer from conjugated polymer to the (benzo)porphyrin was observed in the nanoparticles. The solutions of the conjugated polymers in organic solvents (uncharged polymer precursors in toluene) were further investigated.

Figure 3-11 Dissolved conjugated polymers (left) and conjugated polymer-based nanoparticles (right) under UV light.

The photography images of the toluene solution of a conjugated polyer incorporating PtTFPP in toluene and the dispersion of the positively charged nanoparticles in water (both anoxic) under excitation with a 365-nm line of the UV lamp,

The spectral difference of conjugated polymer and conjugated polymer-based nanoparticles can be seen by a naked eye under UV light (Figure 3-11). It is evident that the energy transfer is very efficient in case of the nanoparticles (virtually no blue emission from the conjugated polymer is visible) but is absent in case of the dissolved polymer (emitting solely blue light). The spectra below (Figure 3-12) confirm the above observation.

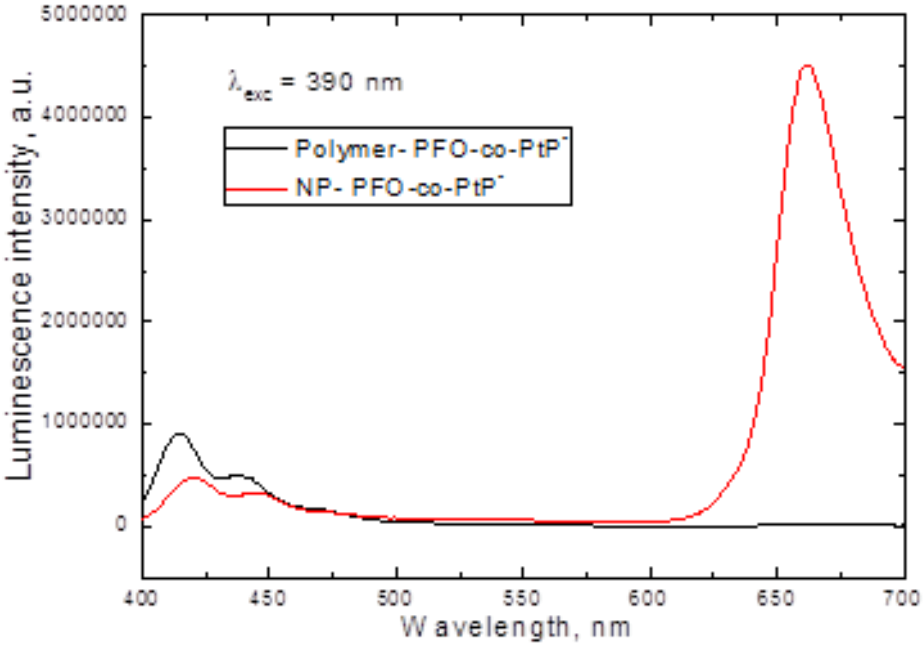

Figure 3-12 Emission spectra of dissolved PtTFPP integrated conjugated polymer and PtTFPP integrated conjugated polymer-based nanoparticles dispersion. (λ_{exc} = 390 nm)

We provide the following explanation for the above phenomenon. The conjugated polymer incorporating integrated PtTFPP has a long linear structure which is preserved in solution (Figure 3-12). The energy transfer from the conjugated polymer to the porphrin

is not efficient, as the effective energy absorption radius cannot cover all conjugated polymer units. FRET mechanism is quite likely since the emission bands of the conjugated polymer and the absorption of the Q-bands of PtTFPP overlap. When the polymeric nanoparticles are formed, the distance between the energy donor conjugated polymer and the energy acceptor porphrin is significantly smaller. Thus, the more efficient energy transfer is realized in this nanoparticles form.

Figure 3-13 Possible configuration of dissolved polymer

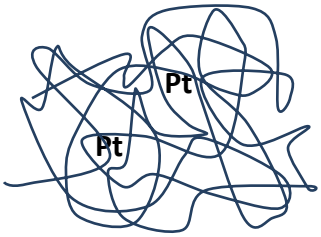

Figure 3-14 Possible configuration of nanoparticles

As observed from Figure 3-15 the same trends are observed for the NIR-emittting conjugated polymer incorporating Pt(II) benzoporphyrin. The same spectral properties are shown in PtTPTtBuBP system above. The oxygen indicator PtTPTBTPF can be excited at 615 nm and has emission at 770 nm wavelength. The corresponding conjugated polymer has excitation and emission wavelength at 460 nm and 550 nm respectively. Virtually no emission can be seen around 770 nm from PtTPTtBuBP integrated conjugated polymer in anoxic toluene solution. On the contrary, huge band at 770-780

nm is observed for the dispersion of PtTPTtBuBP integrated conjugated polymer-based nanoparticles.

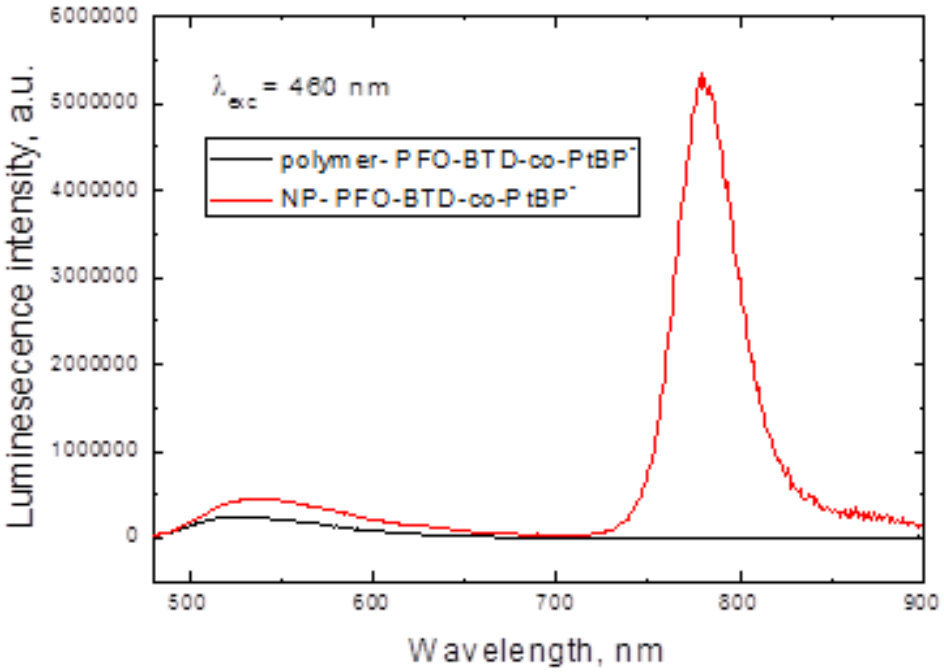

Figure 3-15 Emission spectra of dissolved PtTPTtBuBP integrated conjugated polymer and PtTPTtBuBP integrated conjugated polymer-based nanoparticles dispersion. (λexc = 460 nm)

3.3.4 Decay time of conjugated polymer-based oxygen-sensitive nanoparticles

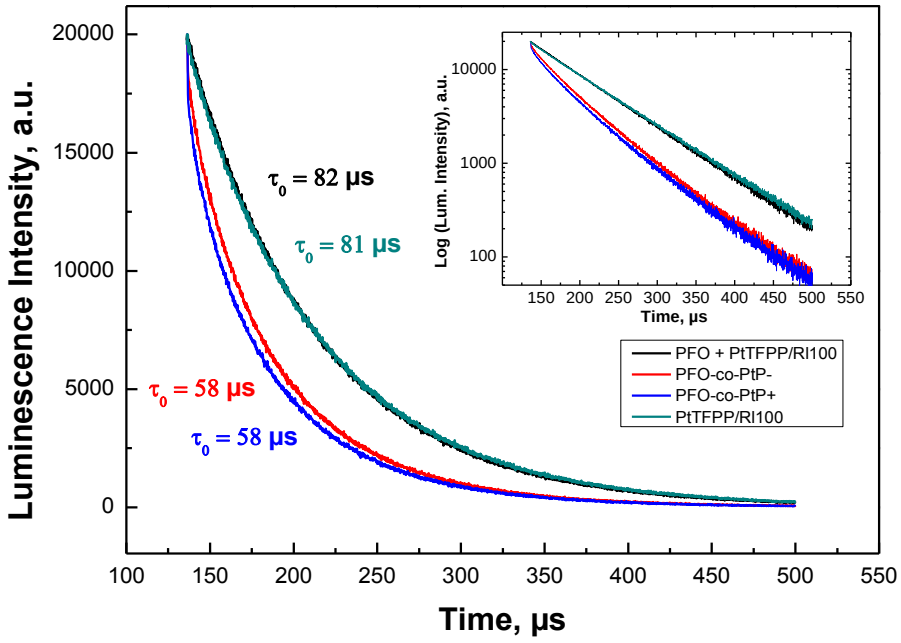

Figure 3-16 Luminescence decay of PtTFPP integrated conjugated polymer-based oxygen sensitive nanoparticles. (The insert shows the logarithmic plots. All measurements were done in deoxygenated dispersions.)

In this part, we compared the decay time of PtTFPP integrated conjugated polymer-based oxygen sensitive nanoparticles with PtTFPP-RL-100 nanoparticles and PFO-PtTFPP-RL-100 nanoparticles. For the PtTFPP system, data is fitted using a mono-exponential fit. The decay time for PtTFPP-RL-100 nanoparticles and PFO-PtTFPP-RL-100 nanoparticles are 81 μs and 82 μs, respectively. The decay time for cationic and anionic PtTFPP integrated conjugated polymer-based nanoparticles is shorter (58 μs). This luminescence intensity decrease in conjugated polymer-based nanoparticles system may be due to the possible quenching of

porphyrin phosphorescence by conjugated polymer. The energy of the triplet state of the conjugated polymers is lower than the energy level of porphrins. So if the porphrin is excited by the energy transferred from conjugated polymers, the emission may diminish due to further triplet-triplet energy transfer to the conjugated polymer. This can explain the shorter decay time of conjugated polymer-based oxygen-sensitive nanoparticles.

Similar trend is observed in case of the Pt(II)-benzoporphyrin-based conjugated polymer particles (Figure 3-17). The shorter decay time has also been observed in PtTPTtBuBP integrated conjugated polymer-based nanoparticles than PtTPTBPF-RL-100 nanoparticles. The data of PtTPTtBuBP conjugated polymer-based nanoparticles are fitted in a two-exponential fit. The decay times of cationic conjugated polymer-based nanoparticles are 41 μs and 15 μs, with the intensity of 83 % and 17 % respectively. For anionic conjugated polymer-based nanoparticles are 40 μs and 14 μs, with the intensity of 82 % and 18 % respectively. On the other hand, the decay profile of PFO-PtTPTBPF-RL-100 nanoparticles is excellently fitted in a mono-exponential fit (τ = 61 μs). The same explanation for PtTFPP system can also be applied here.

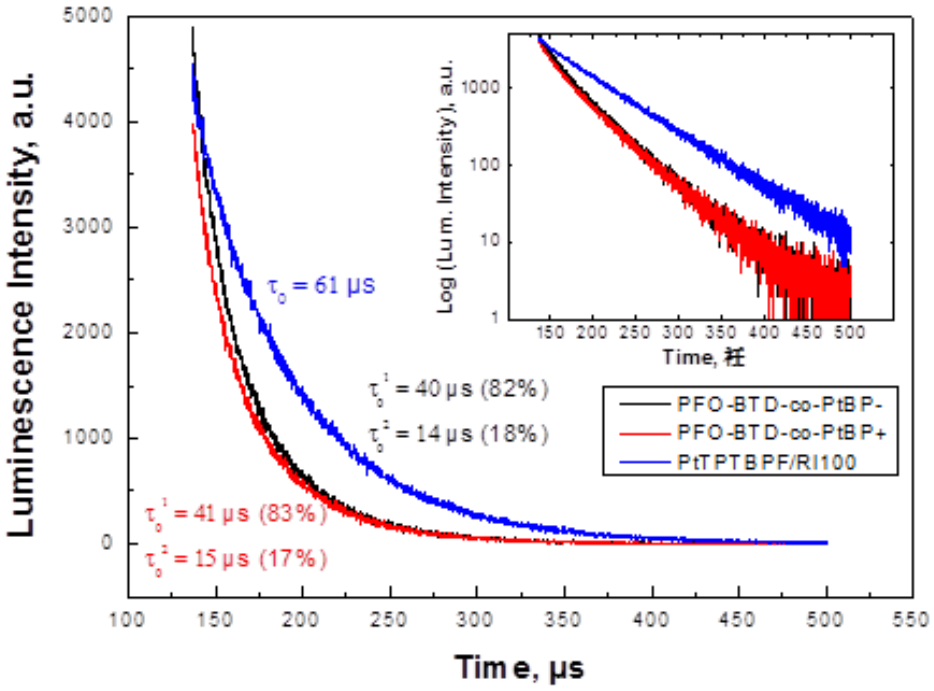

Figure 3-17 Luminescence decay of PtTPTtBuBP integrated conjugated polymer-based oxygen sensitive nanoparticles. (The insert shows the logarithmic plots. All measurements were done in deoxygenated dispersions.)

3.3.5 Oxygen sensitivity of the conjugated polymer-based oxygen-sensitive nanoparticles

The mechanism of oxygen sensors is based on the dynamic quenching of the indicator's luminescence by molecular oxygen. So we compared the spectra of PtTFPP integrated conjugated polymer-based oxygen sensor and PtTPTtBuBP integrated conjugated polymer-based oxygen sensor when they are exposed in air and when deoxygenated.

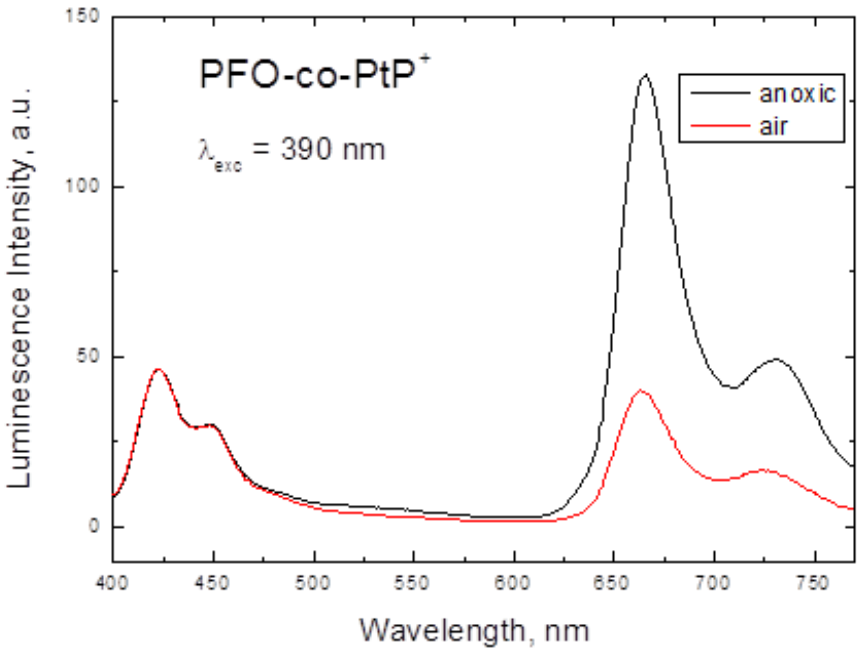

Figure 3-18 Emission spectra of PtTFPP integrated conjugated polymer-based nanoparticle under air saturation and under anoxia condition

For PtTFPP integrated conjugated polymer-based nanoparticle oxygen sensor, we excited it at 390 nm wavelength, which is optimal for conjugated polymer. One can see (Figure 3-18) that luminescence intensity of this oxygen sensor at deoxygenated condition is 3 –

4 times higher than saturated in air. Importantly, the residual blue emission from the conjugated polymer is not affected. Thus, the system is suitable for ratiometric 2-wavelength measurement.

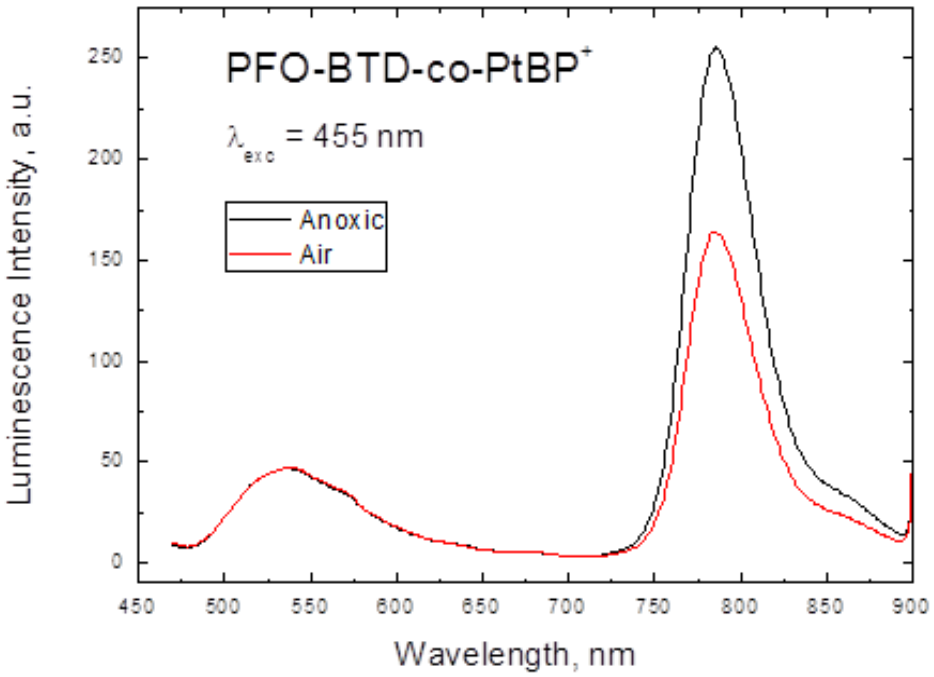

Figure 3-19 Emission spectra of PtTPTtBuBP integrated conjugated polymer-based nanoparticle under air saturation and under anoxia condition

The Pt(II) benzoporphyrin-integrated conjugated polymer nanoparticles show similar behaviour (Figure 3-19). However, the sensitivity is significantly lower than for the PtTFFPP-integrated polymer beads. This is partly due to shorter decay time of the Pt(II) benzoporphyrin, but is also likely that the morphology of the particles is more important here. In fact, the PtTFPP-beads can only be connected twice with the conjugated polymer.

On the other side, up to 4 bonds are possible for PtTPTtBuBP. Thus, the conjugated polymer chains may better shield the oxygen indicator from the quencher.

3.3.6 Particles properties of conjugated polymer-based oxygen-sensitive nanoparticles

Some other characterizations have been done for these 2 categories, 5 kinds of conjugated polymer-based luminescent oxygen-sensitive nanoparticles were investigated.

Table 3-2 Particles properties of conjugated polymer-based oxygen-sensitive nanoparticles

	Z-Ave (d.nm)	Pdl	ZP (mV)
PFO-co-PtP^{+}	35.17	0.249	33.5
PFO-co-PtP^{-}	55.58	0.192	-23.1
PFO-co-PtP$^{+/-}$	37.41	0.192	22.5
PFO-BTD-co-PtBP^{+}	51.78	0.129	33
PFO-BTD-co-PtBP^{-}	49.75	0.094	-23.2

All of these oxygen sensors have small particle size, which is around or below 50 nm. It shows ability for cell penetrating in biological application. Small Pdl value shows the

oxygen sensor particle are quite homogenous in size. Cationic and anionic sensors show positive and negative charges on the particles surface, respectively, which explains their good dispersability in water and ability to interact with different kinds of microorganism. As can be seen, the Zeta-potential of the particles is dependent on the nature of the charged group and is not dependent on the nature of the porphyrin incorporated.

Interestingly, the zeta-potential of zwitterionic conjugated polymer-based nanoparticles is positive. During the synthesis process, we have both positive and negative charged monomers involved. For some reason, the positive charged group is dominant after the nanoparticles synthesis. More study could be done for these "zwitterionic" conjugated polymer-based nanoparticles in real biological system to see the difference with conventional cationic and anionic ones.

3.3.7 Cell penetration ability of conjugated polymer-based oxygen-sensitive nanoparticles

Cell penetration of the particles was investigated by incubating the MEF cells with 10 μg/mL dispersion of the beads for 18h. As can be seen Figure 3-20, the cationc and anionic particles containing copolymerized PtTFPP show excellent uptake by the cells. These particles can be particularly promising for ratiometric imaging of intracellular oxygen. On the contrary, the anionic conjugated polymer particles were shown to remain outside the MEF cells and can be suitable for extracellular imaging of oxygen. The more detailed studies with MEF and other cell cultures are ongoing in the group of Prof. Dmitri Papkovsky in the University College Cork (Ireland).

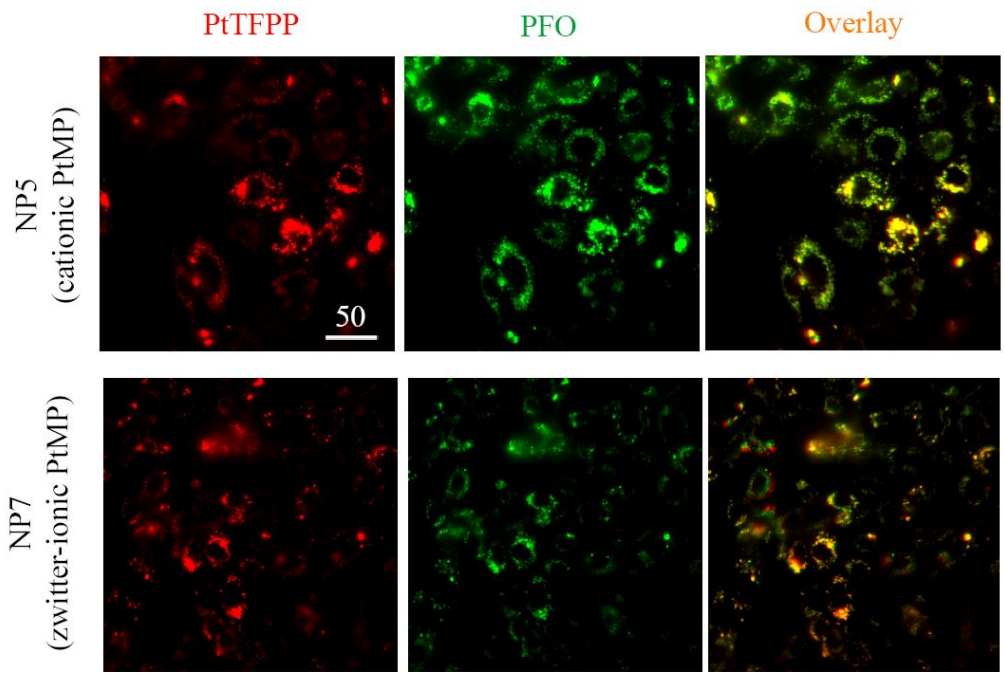

Figure 3-20 Microscopic images of the MEF cells incubated with the cationic and zwitterionic conjugated polymer particles

The oxygen-sensing properties inside the cells and applications are currently investigated together with cooperation partners.

3.4 Summary

In conclusion, this series of conjugated polymer-based oxygen-sensitive nanoparticles were synthesized successfully. The synthetic methodology to incorporate charged functionalities and oxygen-sensitive indicator is established by zeta potential measurement and sir-saturated/ anoxic condition emission excitation spectrum. Conjugated polymers were synthesized by Suzuki coupling, and nanoparticles were prepared through fast precipitate method. All the particles are well dispersible in water.

Efficient energy transfer in particles in contrast to the dissolved polymers was established. Very high brightness, significant enhancement compared to the state-of-the-art beads is observed.

The luminescence of the new nanoparticles is sensitive to oxygen so that they are promising as oxygen-sensitive nano-probes. Also these series optical oxygen sensors are suitable for two-wavelength ratiometric sensing and imaging. Cationic and “zwitterionic” conjugated polymer-based oxygen-sensitive nanoparticles show the ability to penetrate the cells. It is the first time that NIR emitting beads are prepared. They are expected to be particularly promising for tissue applications.

Chapter 4 Conclusion and future work

4.1 Conclusion

Design of polymeric nanoparticles for edible antimicrobials

Plain chitosan nanoparticles synthesized with an optimal concentration of TPP solution were investigated for attachment of antimicrobial peptides on the surface or incorporation during the synthesis process. Alginate, as a bonding layer between two cationic species, chitosan and nisin, shows stable interactions with both of them through electrostatic forces. For polylysine, a different method was used to incorporate it inside of the chitosan nanoparticles. Various mass ratios of chitosan and polylysine in the nanoparticle synthesis solution have been investigated, and the ratio of 10:1 was used in the following experiments.

Chitosan was realized in nanoparticles form for food application use. And the potential synergistic effect of the antimicrobial properties of chitosan and antimicrobial peptide on both Gram positive and Gram negative bacteria are expected to see. Plain chitosan nanoparticles, nisin coated chitosan nanoparticles, and polylysine incorporated chitosan nanoparticles, were prepared for further investigation of antimicrobial effectiveness in Dr. Karl Matthews' group in the Department of Food Science.

Design of polymeric nanoparticles for chemical oxygen sensors

A series of conjugated polymer-based oxygen-sensitive nanoparticles was synthesized successfully. The synthetic methodology to incorporate charged functionalities and an

oxygen-sensitive indicator is established by zeta potential measurements and sir-saturated/ anoxic condition emission excitation spectrum. Conjugated polymers were synthesized by Suzuki coupling, and nanoparticles were prepared through the fast precipitate method. All the particles are well dispersible in water.Efficient energy transfer in particles in contrast to the dissolved polymers was established. Very high brightness, significant enhancement compared to the state-of-the-art beads is observed.

4.2 Future work

Design of polymeric nanoparticles for edible antimicrobials

Besides nisin and polylysine, other antimicrobial peptides can be investigated for incorporation with chitosan nanoparticles to form stable, effective and efficient antimicrobial agents in order to eliminate pathogenic bacteria and reduce the total population of bacteria during food processing.

The antimicrobial properties of chitosan-based nanoparticles have only been tested at the laboratory level. To understand the scalability of it, reduced-scale application assays need to be done. For example, the antimicrobial activity can be tested on fresh produce, such as tomatoes, lettuce, and mangoes. And a washing process can be conducted with our nanoparticles, chlorinated water, and a combination of two to see whether or not the chitosan-based nanoparticles antimicrobial performs synergistic or antagonistic effects.

With the globalization of the food supply, the demand for prolonging the shelf-life of fresh produce is increasing. Another application for these chitosan-based nanoparticles antimicrobials is to prolong the shelf-life of fresh/ fresh-cut produce.

Design of polymeric nanoparticles for chemical oxygen sensors

The luminescence of the new nanoparticles is sensitive to low concentrations of oxygen in biological systems. The lowest measureable concentration can be determined. Also these series optical oxygen sensors are suitable for two-wavelength ratiometric sensing and imaging. Cationic and “zwitterionic” conjugated polymer-based oxygen-sensitive nanoparticles show the ability to penetrate the cells. It is the first time that NIR emitting

beads are prepared. They are expected to be particularly promising for tissue applications. More application can be investigated in microfluidic systems.

References

1. Braden, C.R. and R.V. Tauxe, *Emerging Trends in Foodborne Diseases.* Infectious disease clinics of North America, 2013. **27**(3): p. 517-533.
2. Farkas, J., *Irradiation as a method for decontaminating food: a review.* International Journal of Food Microbiology, 1998. **44**(3): p. 189-204.
3. Dey, M., et al., *Recalls of Foods due to Microbiological Contamination Classified by the US Food and Drug Administration, Fiscal Years 2003 through 2011.* Journal of Food Protection®, 2013. **76**(6): p. 932-938.
4. McEntire, J., *Foodborne Disease: The Global Movement of Food and People.* Infectious disease clinics of North America, 2013. **27**(3): p. 687-693.
5. Lynch, M., R. Tauxe, and C. Hedberg, *The growing burden of foodborne outbreaks due to contaminated fresh produce: risks and opportunities.* Epidemiology and infection, 2009. **137**(03): p. 307-315.
6. Devlieghere, F., L. Vermeiren, and J. Debevere, *New preservation technologies: possibilities and limitations.* International Dairy Journal, 2004. **14**(4): p. 273-285.
7. YUSTE, J., et al., *HIGH PRESSURE PROCESSING FOR FOOD SAFETY AND PRESERVATION: A REVIEW1.* Journal of Rapid Methods & Automation in Microbiology, 2001. **9**(1): p. 1-10.
8. Góngora-Nieto, M., et al., *Food processing by pulsed electric fields: treatment delivery, inactivation level, and regulatory aspects.* LWT-Food Science and Technology, 2002. **35**(5): p. 375-388.
9. Wheeldon, I., et al., *Nanoscale tissue engineering: spatial control over cell-materials interactions.* Nanotechnology, 2011. **22**(21): p. 212001.
10. Kievit, F.M. and M. Zhang, *Surface engineering of iron oxide nanoparticles for targeted cancer therapy.* Accounts of chemical research, 2011. **44**(10): p. 853-862.
11. Kugel, A., S. Stafslien, and B.J. Chisholm, *Antimicrobial coatings produced by "tethering" biocides to the coating matrix: a comprehensive review.* Progress in Organic Coatings, 2011. **72**(3): p. 222-252.
12. Fathi, M., M. Mozafari, and M. Mohebbi, *Nanoencapsulation of food ingredients using lipid based delivery systems.* Trends in food science & technology, 2012. **23**(1): p. 13-27.
13. Donsì, F., et al., *Design of nanoemulsion-based delivery systems of natural antimicrobials: effect of the emulsifier.* Journal of biotechnology, 2012. **159**(4): p. 342-350.
14. Helander, I., et al., *Chitosan disrupts the barrier properties of the outer membrane of Gram-negative bacteria.* International Journal of Food Microbiology, 2001. **71**(2): p. 235-244.
15. Larsen, M.U., et al., *Biocompatible nanoparticles trigger rapid bacteria clustering.* Biotechnology progress, 2009. **25**(4): p. 1094-1102.
16. Tripathi, M.M., et al., *An optical sensor for multi-species impurity monitoring in hydrogen fuel.* Sensors and Actuators B: Chemical, 2012. **171**: p. 416-422.

17. John, G.T., et al., *Integrated optical sensing of dissolved oxygen in microtiter plates: a novel tool for microbial cultivation.* Biotechnology and bioengineering, 2003. **81**(7): p. 829-836.
18. Wolfbeis, O.S., *Fiber optic chemical sensors and biosensors*. Vol. 1. 1991: CRC press Boca Raton, FL.
19. Nei, L. and R.G. Compton, *An improved Clark-type galvanic sensor for dissolved oxygen.* Sensors and Actuators B: Chemical, 1996. **30**(2): p. 83-87.
20. Amao, Y., *Probes and polymers for optical sensing of oxygen.* Microchimica Acta, 2003. **143**(1): p. 1-12.
21. Freeman, T.M. and W.R. Seitz, *Oxygen probe based on tetrakis (alkylamino) ethylene chemiluminescence.* Analytical chemistry, 1981. **53**(1): p. 98-102.
22. Wolfbeis, O.S., et al., *Fiber-optic fluorosensor for oxygen and carbon dioxide.* Analytical chemistry, 1988. **60**(19): p. 2028-2030.
23. Skoog, D., D. West, and F. Holler, *Fundamentals of Analytical Chemistry (5th edn.) Saunders College.* New York, 1988.
24. McDonagh, C., C.S. Burke, and B.D. MacCraith, *Optical chemical sensors.* Chemical reviews, 2008. **108**(2): p. 400-422.
25. Quaranta, M., S. Borisov, and I. Klimant, *Indicators for optical oxygen sensors.* Bioanalytical Reviews, 2012. **4**(2-4): p. 115-157.
26. Lee, Y.-E.K., R. Kopelman, and R. Smith, *Nanoparticle PEBBLE sensors in live cells and in vivo.* Annual review of analytical chemistry (Palo Alto, Calif.), 2009. **2**: p. 57.
27. Fercher, A., et al., *Intracellular O2 sensing probe based on cell-penetrating phosphorescent nanoparticles.* Acs Nano, 2011. **5**(7): p. 5499-5508.
28. Xu, H., et al., *A real-time ratiometric method for the determination of molecular oxygen inside living cells using sol-gel-based spherical optical nanosensors with applications to rat C6 glioma.* Analytical chemistry, 2001. **73**(17): p. 4124-4133.
29. Wu, C., et al., *Ratiometric single-nanoparticle oxygen sensors for biological imaging.* Angewandte Chemie, 2009. **48**(15): p. 2741-5.
30. Koo Lee, Y.-E., et al., *Near infrared luminescent oxygen nanosensors with nanoparticle matrix tailored sensitivity.* Analytical chemistry, 2010. **82**(20): p. 8446-8455.
31. Kondrashina, A.V., et al., *A Phosphorescent Nanoparticle-Based Probe for Sensing and Imaging of (Intra)Cellular Oxygen in Multiple Detection Modalities.* Advanced Functional Materials, 2012. **22**(23): p. 4931-4939.
32. Coogan, M.P., et al., *Probing intracellular oxygen by quenched phosphorescence lifetimes of nanoparticles containing polyacrylamide-embedded [Ru (dpp (SO3Na) 2) 3] Cl2.* Photochemical & photobiological sciences, 2010. **9**(1): p. 103-109.
33. Dodane, V. and V.D. Vilivalam, *Pharmaceutical applications of chitosan.* Pharmaceutical Science & Technology Today, 1998. **1**(6): p. 246-253.
34. Paul, W. and C. Sharma, *Chitosan, a drug carrier for the 21st century: a review.* STP pharma sciences, 2000. **10**(1): p. 5-22.
35. Lehr, C.-M., et al., *In vitro evaluation of mucoadhesive properties of chitosan and some other natural polymers.* International journal of Pharmaceutics, 1992. **78**(1): p. 43-48.

36. Yu, K., et al., *Copper ion adsorption by chitosan nanoparticles and alginate microparticles for water purification applications.* Colloids and Surfaces A: Physicochemical and Engineering Aspects, 2013. **425**: p. 31-41.
37. Schmuhl, R., H. Krieg, and K. Keizer, *Adsorption of Cu (II) and Cr (VI) ions by chitosan: Kinetics and equilibrium studies.* Water Sa, 2004. **27**(1): p. 1-8.
38. Reddad, Z., et al., *Adsorption of several metal ions onto a low-cost biosorbent: kinetic and equilibrium studies.* Environmental science & technology, 2002. **36**(9): p. 2067-2073.
39. Hirano, S., et al., *Chitosan: a biocompatible material for oral and intravenous administrations*, in *Progress in biomedical polymers*1990, Springer. p. 283-290.
40. Weiner, M., *An overview of the regulatory status and of the safety of chitin and chitosan as food and pharmaceutical ingredients.* Advances in chitin and chitosan, 1992: p. 663-670.
41. Arai, K., T. Kinumaki, and T. Fujita, *Toxicity of chitosan.* Bull. Tokai. Region. Fish. Res. Lab., 1968(56): p. 89-94.
42. Shahidi, F., J.K.V. Arachchi, and Y.-J. Jeon, *Food applications of chitin and chitosans.* Trends in food science & technology, 1999. **10**(2): p. 37-51.
43. Devlieghere, F., A. Vermeulen, and J. Debevere, *Chitosan: antimicrobial activity, interactions with food components and applicability as a coating on fruit and vegetables.* Food Microbiology, 2004. **21**(6): p. 703-714.
44. No, H.K., et al., *Antibacterial activity of chitosans and chitosan oligomers with different molecular weights.* International Journal of Food Microbiology, 2002. **74**(1): p. 65-72.
45. Azadi, G., et al., *Improved antimicrobial potency through synergistic action of chitosan microparticles and low electric field.* Applied biochemistry and biotechnology, 2012. **168**(3): p. 531-541.
46. Neidhardt, F.C., et al., *Escherichia coli and Salmonella: cellular and molecular biology.* 1996.
47. Mi, F.L., et al., *Kinetic study of chitosan‐tripolyphosphate complex reaction and acid‐resistive properties of the chitosan‐tripolyphosphate gel beads prepared by in‐liquid curing method.* Journal of Polymer Science Part B: Polymer Physics, 1999. **37**(14): p. 1551-1564.
48. Mi, F.-L., et al., *Synthesis and characterization of biodegradable TPP/genipin co-crosslinked chitosan gel beads.* Polymer, 2003. **44**(21): p. 6521-6530.
49. Klöck, G., et al., *Biocompatibility of mannuronic acid-rich alginates.* Biomaterials, 1997. **18**(10): p. 707-713.
50. Mi, F.-L., H.-W. Sung, and S.-S. Shyu, *Drug release from chitosan–alginate complex beads reinforced by a naturally occurring cross-linking agent.* Carbohydrate Polymers, 2002. **48**(1): p. 61-72.
51. Orive, G., et al., *Biocompatibility of microcapsules for cell immobilization elaborated with different type of alginates.* Biomaterials, 2002. **23**(18): p. 3825-3831.
52. Lai, H.L., A. Abu'Khalil, and D.Q. Craig, *The preparation and characterisation of drug-loaded alginate and chitosan sponges.* International journal of Pharmaceutics, 2003. **251**(1): p. 175-181.

53. Ramesh Babu, V., et al., *Preparation of sodium alginate–methylcellulose blend microspheres for controlled release of nifedipine.* Carbohydrate Polymers, 2007. **69**(2): p. 241-250.
54. Moe, S., K. Dragel, and O. Smidsrød, *Alginates In: Stephen, A. M. editor*. Food Polysaccharides and Their Applications.
55. Steinbüchel, A. and S.K. Rhee, *Polysaccharides and polyamides in the food industry: properties, production, and patents*2005: Wiley-VCH Verlag GmbH & CO. KGaA.
56. Fejerskov, O. and E. Kidd, *Dental caries: the disease and its clinical management*2008: John Wiley & Sons.
57. Begde, D., et al., *Immunomodulatory efficacy of nisin—a bacterial lantibiotic peptide.* Journal of peptide science, 2011. **17**(6): p. 438-444.
58. Karam, L., et al., *Study of surface interactions between peptides, materials and bacteria for setting up antimicrobial surfaces and active food packaging.*
59. Food and D. Administration, *Nisin preparation: affirmation of GRAS status as a direct human food ingredient.* Federal Register, 1988. **53**(11): p. 247-11.
60. Hansen, J.N., *Antibiotics synthesized by posttranslational modification.* Annual Reviews in Microbiology, 1993. **47**(1): p. 535-564.
61. Breukink, E. and B. de Kruijff, *Lipid II as a target for antibiotics.* Nature Reviews Drug Discovery, 2006. **5**(4): p. 321-323.
62. Severina, E., A. Severin, and A. Tomasz, *Antibacterial efficacy of nisin against multidrug-resistant Gram-positive pathogens.* Journal of Antimicrobial Chemotherapy, 1998. **41**(3): p. 341-347.
63. Hiraki, J., et al., *Use of ADME studies to confirm the safety of ε-polylysine as a preservative in food.* Regulatory Toxicology and Pharmacology, 2003. **37**(2): p. 328-340.
64. Health, M.o., et al., *Health and welfare statistics in Japan*1987: Health and Welfare Statistics Association.
65. Shima, S., et al., *Antimicrobial action of epsilon-poly-L-lysine.* The Journal of antibiotics, 1984. **37**(11): p. 1449-1455.
66. Zhang, H., et al., *Monodisperse chitosan nanoparticles for mucosal drug delivery.* Biomacromolecules, 2004. **5**(6): p. 2461-2468.
67. Fernandez, M.J.A., et al., *Application of nanoparticles based on hydrophilic polymers as pharmaceutical forms*, 2003, Google Patents.
68. Roy, K., et al., *Oral gene delivery with chitosan–DNA nanoparticles generates immunologic protection in a murine model of peanut allergy.* Nature medicine, 1999. **5**(4): p. 387-391.
69. Calvo, P., et al., *Novel hydrophilic chitosan-polyethylene oxide nanoparticles as protein carriers.* Journal of Applied Polymer Science, 1997. **63**(1): p. 125-132.
70. Banerjee, T., et al., *Preparation, characterization and biodistribution of ultrafine chitosan nanoparticles.* International journal of Pharmaceutics, 2002. **243**(1): p. 93-105.
71. Larsen, M.U. and N.C. Shapley. *Tailoring The Size, Surface Charge, And Release Properties Of Biocompatible Chitosan Nanoparticles*. in *The 2007 Annual Meeting*. 2007.

72. No, H., et al., *Applications of chitosan for improvement of quality and shelf life of foods: a review.* Journal of Food Science, 2007. **72**(5): p. R87-R100.
73. Nagpal, K., S.K. Singh, and D.N. Mishra, *Chitosan nanoparticles: a promising system in novel drug delivery.* Chem Pharm Bull (Tokyo), 2010. **58**(11): p. 1423-1430.
74. Ouattara, B., et al., *Diffusion of Acetic and Propionic Acids from Chitosan - based Antimicrobial Packaging Films.* Journal of Food Science, 2000. **65**(5): p. 768-773.
75. Blum, L.J. and L. Blum, *Bio-and chemi-luminescent sensors*1997: World Scientific.
76. Gründler, P., *Chemical sensors: an introduction for scientists and engineers*2007: Springer.
77. Borisov, S.M. and O.S. Wolfbeis, *Optical biosensors.* Chemical reviews, 2008. **108**(2): p. 423-461.
78. Tang, B., et al., *A near-infrared neutral pH fluorescent probe for monitoring minor pH changes: imaging in living HepG2 and HL-7702 cells.* Journal of the American Chemical Society, 2009. **131**(8): p. 3016-3023.
79. Larsen, M., et al., *A simple and inexpensive high resolution color ratiometric planar optode imaging approach: application to oxygen and pH sensing.* Limnol. Oceanogr.: Methods, 2011. **9**: p. 348-360.
80. Arain, S., et al., *Characterization of microtiterplates with integrated optical sensors for oxygen and pH, and their applications to enzyme activity screening, respirometry, and toxicological assays.* Sensors and Actuators B: Chemical, 2006. **113**(2): p. 639-648.
81. Schouest, K., et al., *Toxicological assessment of chemicals using Caenorhabditis elegans and optical oxygen respirometry.* Environmental toxicology and chemistry, 2009. **28**(4): p. 791-799.
82. Mills, A., *Oxygen indicators and intelligent inks for packaging food.* Chemical Society Reviews, 2005. **34**(12): p. 1003-1011.
83. Nagl, S. and O.S. Wolfbeis, *Classification of chemical sensors and biosensors based on fluorescence and phosphorescence,* in *Standardization and Quality Assurance in Fluorescence Measurements I*2008, Springer. p. 325-346.
84. Baldini, F., et al., *Optical chemical sensors*. Vol. 224. 2006: Springer.
85. Lobnik, A., et al., *pH optical sensors based on sol–gels: chemical doping versus covalent immobilization.* Analytica chimica acta, 1998. **367**(1): p. 159-165.
86. Wang, X.-D. and O.S. Wolfbeis, *Fiber-optic chemical sensors and biosensors (2008–2012).* Analytical chemistry, 2012. **85**(2): p. 487-508.
87. Carraway, E., et al., *Photophysics and photochemistry of oxygen sensors based on luminescent transition-metal complexes.* Analytical chemistry, 1991. **63**(4): p. 337-342.
88. Dunphy, I., S.A. Vinogradov, and D.F. Wilson, *Oxyphor R2 and G2: phosphors for measuring oxygen by oxygen-dependent quenching of phosphorescence.* Analytical biochemistry, 2002. **310**(2): p. 191-198.
89. Vogel, A. and V. Venugopalan, *Mechanisms of pulsed laser ablation of biological tissues.* Chemical reviews, 2003. **103**(2): p. 577-644.

90. Patil, A., A. Heeger, and F. Wudl, *Optical properties of conducting polymers.* Chemical reviews, 1988. **88**(1): p. 183-200.
91. Kajzar, F., et al., *< i> X</i>< sup>(3)</sup> of trans-(CH)< sub> x</sub>: Experimental observation of 2A< sub> g</sub> excited state.* Synthetic Metals, 1987. **17**(1): p. 563-567.
92. Schmitt-Rink, S., D. Miller, and D.S. Chemla, *Theory of the linear and nonlinear optical properties of semiconductor microcrystallites.* Physical Review B, 1987. **35**(15): p. 8113.
93. Marder, S.R., J.E. Sohn, and G.D. Stucky, *Materials for Nonlinear Optics Chemical Perspectives*, 1991, DTIC Document.
94. Sailor, M.J., et al., *Thin films of n-Si/poly-(CH3) 3Si-cyclooctatetraene: conducting-polymer solar cells and layered structures.* Science, 1990. **249**(4973): p. 1146-1149.
95. Burroughes, J., et al., *Light-emitting diodes based on conjugated polymers.* nature, 1990. **347**(6293): p. 539-541.
96. Bradley, D., *Conjugated polymer electroluminescence.* Synthetic Metals, 1993. **54**(1): p. 401-415.
97. McQuade, D.T., A.E. Pullen, and T.M. Swager, *Conjugated polymer-based chemical sensors.* Chemical reviews, 2000. **100**(7): p. 2537-2574.
98. Borisov, S.M., et al., *Precipitation as a simple and versatile method for preparation of optical nanochemosensors.* Talanta, 2009. **79**(5): p. 1322-1330.
99. Buck, S.M., et al., *Optochemical nanosensor PEBBLEs: photonic explorers for bioanalysis with biologically localized embedding.* Current opinion in chemical biology, 2004. **8**(5): p. 540-546.
100. Dmitriev, R.I., et al., *Assessment of cellular oxygen gradients with a panel of phosphorescent oxygen-sensitive probes.* Analytical chemistry, 2012. **84**(6): p. 2930-2938.
101. Pu, K.Y., Z. Fang, and B. Liu, *Effect of charge density on energy - transfer properties of cationic conjugated polymers.* Advanced Functional Materials, 2008. **18**(8): p. 1321-1328.